DESIGN OF A PROTOTYPE RECEPTOR-CENTRIC DECISION SUPPORT SYSTEM FOR STUDYING THE IMPACT OF HYPOTHETICAL NUCLEAR ACCIDENTS & THEIR MITIGATION

A Thesis

by

ARSHAD MOHAMED ALI

Submitted to the Graduate and Professional School of
Texas A&M University
in partial fulfillment of the requirements for the degree of

MASTER OF SCIENCE

Chair of Committee,	Konstantinos E. Kakosimos
Committee Members,	Luc Vechot
	Zohreh Eslami
	Othmane Bouhali
Head of Department,	Arul Jayaraman

August 2021

Major Subject: Chemical Engineering

ABSTRACT

Major nuclear accidents such as Chernobyl and Fukushima-Daiichi have highlighted the need for robust consequence assessment and countermeasure (mitigation) plans. As such, FEMA provides several planning fundamentals such as ‘community-based planning’ and ‘considering all hazards and threats’. However, specific guidance on the implementation of these fundamentals was not found in the reviewed literature. Thus, a prototype DSS in line with these fundamentals was created to study the consequences of nuclear accidents and suggest countermeasures. A ‘receptor-centric’ framework was proposed to implement community-based planning. Similarly, a data-driven framework with stratified random sampling for release times throughout the year was applied to study a larger number of accident scenarios. This sampling approach was more robust than the wind rose approach in capturing a greater spectrum of possible impacts. The need for sufficient accident sampling was also demonstrated. Non-simultaneous individual accidents in regions with multiple nuclear plants were studied as no corresponding methodology was found in the literature. Time-dependent source terms were used to improve accuracy.

The DSS was tested on Qatar for hypothetical accidents at Barakah, Bushehr, and Umm Huwayd plants for the year 2017. All results were compared for 25 secondary receptors over seven categories. These accidents were determined to potentially cause both short-term and long-term health impacts, with ingestion exposure being the critical pathway. Thus, agricultural countermeasures were chosen as the core countermeasure

strategy. Inhalation and groundshine exposure were also identified as pathways of concern. Mesaieed industrial area and Dukhan oil fields were determined to be disproportionately affected by nuclear accidents. Based on radioactive cloud spread, strategies for placement of early warning sensors were also proposed. Sheltering and food restrictions were chosen based on consequence assessment. A novel visualization method was used to guide food restrictions. An insufficient sampling rate hampered a complete comparison of the base case and countermeasure case. Nonetheless, the proposed countermeasure strategy was determined to be inadequate, requiring stricter measures to protect the population.

Various avenues for future research were identified, including further DSS development, module, and data improvements. The proposed design is expected to facilitate the development of similar DSS for harmful airborne releases.

ACKNOWLEDGEMENTS

First and foremost, I would like to thank Allah the Almighty for his grace and blessings, without which I would never have accomplished this work. By his blessings, I obtained the QNRF-GSRA fund, which many thought nearly impossible, and which enabled this work. Furthermore, he blessed me with the right resources, mentors, and skills to carry out a project on a topic in which I have no previous experience.

Next, I would like to thank my committee chair, Dr. Konstantinos, for his guidance, support, and encouragement throughout the project and for providing me the idea for such a unique topic. I am thankful for Dr. Konstantinos's taking time to meet me regularly and give me feedback on my progress.

I want to thank Dr. Vechot and MKOPSC for their advice in the ideation phase, which helped refine the focus of my thesis.

I also appreciate Dr. Eslami, and Dr. Bouhali, for their support throughout this research.

I would like to thank Karlsruhe Institute of Technology (KIT)/JRODOS team for their help in the software installation and initial debugging.

I would also like to express my appreciation to my friends for their support throughout the thesis and for making the degree more memorable, especially during the lockdowns and difficulties of COVID 19.

Thanks also go to my colleagues and the department faculty and staff for making my time at Texas A&M University a great experience.

Finally, a deep appreciation to my family, especially my mother and father for their encouragement, love, and support during these trying times.

CONTRIBUTORS AND FUNDING SOURCES

Contributors

This work was supervised by a thesis committee consisting of Professor Kakosimos Konstantinos [advisor] and Professor Luc Vechot of the Chemical Engineering Program at TAMUQ, Professor Othmane Bouhali of the Science Program at TAMUQ, and Professor Zohreh Eslami of the Liberal Arts Program at TAMUQ and Educational Psychology at TAMU.

Dr. Hala Hassan provided the land use, soil classification, and population density maps.

The software JRODOS used in the project was provided by Karlsruhe Institute of Technology (KIT).

All other work conducted for this thesis was completed by the student independently.

Funding Sources

This thesis was made possible by the award GSRA6-2-0612-19081 from Qatar National Research Fund (a member of Qatar Foundation). The contents herein are solely the responsibility of the author.

NOMENCLATURE

ARS	Acute Radiation Syndrome
DSS	Decision Support System
EEZ	Exclusive Economic Zone
ERP	Emergency Response Plan
FAO	Food and Agriculture Organization (United Nations)
FDMT	Terrestrial Food Chain and Dose Module
FEMA	Federal Emergency Management Agency
FP	Fission Product
FRM	Food Restriction Metric
GIS	Geographic Information System
GL	Guideline Level
HEIS	Household Expenditure and Income Survey
ICRP	International Commission on Radiological Protection
LOCA	Loss of Cooling Accident
NOAA	National Oceanic and Atmospheric Administration
NPP	Nuclear Power Plant
NRC	Nuclear Regulatory Commission (USA)
NWP	Numerical Weather Prediction
PWR	Pressurized Water Reactor

SRM	Stratified Random Sampling
USDA	United States Department of Agriculture
WHO	World Health Organization
WRB	World Reference Base for soil resource

TABLE OF CONTENTS

Page

LIST OF FIGURES

Page

LIST OF TABLES

Page

1. INTRODUCTION

Several nuclear accidents with varying consequences have occurred around the world since 1952. The Chernobyl, Three-mile island and Fukushima Daiichi accidents are most widely known due to their significant impact (LAKA Foundation; Datablog, 2011). These accidents, especially the one at Fukushima Daiichi, have highlighted the importance of an effective and versatile emergency response plan (ERP) to mitigate the consequences of a nuclear accident (Funabashi and Kitazawa, 2012).

A robust consequence assessment and countermeasure (mitigation measures) plan are needed to create an effective ERP. (FEMA, 2010). To aid in this endeavor, the US Federal Emergency Management Agency (FEMA) provides several planning fundamentals. One such fundamental is to use ‘community-based planning’ to account for the needs and diversity within the population. This approach is essential to minimize both the short-term and long-term impact on all sections of society and the regional economy. Different regional areas, population segments, demographics will require various mitigation measures. For example, if most of the population does not own cars, individual evacuation would not be feasible (FEMA, 2010). Similarly, the country's critical infrastructure, such as desalination plants, oil fields, and transport hubs, cannot be entirely and suddenly abandoned. Instead, these require a planned and systematic approach to minimize disruption while protecting workers from any hazards.

Another important fundamental is to ‘consider all hazards and threats’ to develop flexible & scalable solutions for disaster management (FEMA, 2010). Such a plan is

required to ensure that the broader consequences of the emergency response, such as economic cost and social disruption, do not outweigh the expected benefits to the population (Brown et al., 2007). Furthermore, when one considers all hazards, similarities between emergency responses can be seen. Creating mitigation plans based on these similarities can ease implementing these plans since all responders will have sufficient training in these measures (FEMA, 2010). While one can see the importance of these guidelines, the exact method of implementing these guidelines in consequence assessment and countermeasure planning remains vague. Consequently, studies on hypothetical nuclear accidents were reviewed below to examine the implementation of these guidelines in practice.

1.1. Literature Review

Several authors worldwide have studied the impact of hypothetical nuclear accidents. For example, Liland et. al predicted the health and environmental impact of a hypothetical nuclear accident from the Sellafield nuclear plant (UK) on Norway. This study used a chain of models similar to a decision support system (DSS) for their predictions (Liland et al., 2020). This study builds on an earlier study by Ytre-Eide et. al for the same Sellafield plant (Ytre-Eide et al., 2009). Likewise, Aliyu et al. estimated the collective effective dose and lifetime cancer risk resulting from standard operational releases and releases during a hypothetical accident at a proposed NPP in Nigeria (Aliyu et al., 2014; Aliyu et al., 2015).

Min et al. studied the individual effective dose and cancer risk due to an accident at Haiyang NPP in China on the Korean peninsula (Min and Kim, 2018), while Tang et al. included mainland China and the Korean peninsula in their analysis (Tang et al., 2020). In contrast, Dvorzhak conducted a level 3 probabilistic risk assessment for a hypothetical nuclear plant focusing on carrying out a large number of simulations. The study aimed to determine the most likely dose to estimate the risk of an NPP installation (Dvorzhak et al., 2016).

A more considerable number of studies were found for the Middle East region, possibly due to the geopolitical concerns behind the use of nuclear power within the region (Ebel, 2010). The exponential increase in NPPs within the region is best illustrated in Figure 2 below. The majority of the studies have been conducted to understand the risk to the population in case of releases during standard operation (Sohrabi et al., 2013b; Pirouzmand et al., 2015) and accidents (Raisali et al., 2006; Sohrabi et al., 2013a; Beeley and Kim, 2014; Pirouzmand et al., 2015) from the Bushehr plant in Iran. Apart from Bushehr, accidents at Barakah NPP in UAE (Beeley and Kim, 2014) and a hypothetical NPP in Iraq (Mohammed Saeed et al., 2020) were also studied. Interested readers can also refer to other similar studies for hypothetical nuclear accidents and their impacts on countries such as Ghana (Gyamfi et al., 2020), China (Poon et al., 1997; Li et al., 2012), and Malaysia (Shamsuddin et al., 2017).

A detailed look at the above studies reveals some interesting themes. First, most of the studies are ‘plant-centric’ as they center their analysis on the NPP except for Min et.

al, Liland et. al, and Ytre-Eide et. al (Ytre-Eide et al., 2009; Min and Kim, 2018; Liland et al., 2020). This approach is useful for studying the risk of proposed plants for the surrounding communities. However, this approach ignores the diversity in the various receptors (cities, industrial areas), which impacts the dosage profile significantly. This approach contrasts with FEMA's recommendation to use 'community-based planning'.

Secondly, most studies pick specific days of the years to simulate accidents and use the results to analyze the disaster's impact. While helpful to plan for the worst-case disaster, this approach leads to a non-versatile consequence assessment as they fail to account for source terms and weather variations. As a result, this approach contrasts with FEMA's recommendation to consider all hazards and threats during the planning phase.

Thirdly, all the above studies only focus on accidents from one NPP and do not consider combining data for accidents at different NPPs. Finally, all the studies use a non time-dependent source term as part of their simulations. Thus, from the studies above, no straightforward method to implement FEMA guidelines was found.

1.2. Project Objectives and Description

In the absence of a clear method to implement FEMA guidelines in literature, this study explores how these fundamental planning guidelines can be applied to consequence assessment for nuclear accidents and the subsequent countermeasure plan. In addition, this study also explores how a consequence assessment can be done for regions with multiple NPPs. Thus, the study aims the answer the following questions:

1. What is the common impact of individual non-simultaneous radioactive releases in regions with multiple NPPs for a selected area?
2. How can mitigation measures be qualitatively chosen from these common insights?
3. Are these mitigation measures effective in reducing radiation exposure to acceptable limits across all receptors irrespective of NPP considered?

The study answers these questions by creating and utilizing a prototype DSS. For this study, a DSS is defined as a chain of models/algorithms connected under one information system like the definition used by Lim et. al (Lim et al., 2005). This DSS aims to perform complex calculations with simpler inputs to enable quick and accurate decision-making.

To incorporate FEMA's 'community-based planning' recommendation, a 'receptor-centric' framework was used to visualize and analyze the results. A receptor is defined as a unit of analysis that is assumed to consist of several subunits. The smallest/most basic subunit is considered to have homogenous characteristics. For example, a country is a primary receptor that consists of secondary receptors such as cities, industries, desalination plants. The secondary receptor can be further split into districts, groups of humans, individual human beings. As a result, there is a greater focus on improving the data associated with every subunit to improve result accuracy. Furthermore, the aim is to derive shared insights from the impacts of individual non-simultaneous nuclear accidents

on a receptor. It is expected that this bottom-up approach to consequence assessment will facilitate the creation of scalable & flexible ERPs with appropriate plans for each receptor.

Similarly, to incorporate FEMA's recommendation of considering all hazards during planning, a 'data-driven' framework was used. In addition to looking at individual accidents from multiple NPPs, the radioactive cloud dispersion from each NPP was estimated for different accident start times throughout the year. This approach aims to capture the effect of weather variations on cloud dispersion from source to receptor. Implementation of other FEMA guidelines such as stakeholder outreach, analytical problem solving has also been accounted for in this project. Finally, time-dependent source terms were used to improve the accuracy of the results.

As no studies were found for the State of Qatar, the DSS was created and tested for Qatar. Thus, this project contributes to the scientific community at large while improving the regional knowledge database.

The thesis is split into two main sections corresponding to the three objectives mentioned above. The first section (Impact Assessment) aims to answer the first question posed above. This section also contains a description of most DSS modules, such as receptor definition, source term estimation, and cloud dispersion. The second section (Countermeasure Plan) aims to answer the second and third questions posed above. The

complete structure of the DSS is illustrated in Figure 1 below. Boxes of one color are part of the same module.

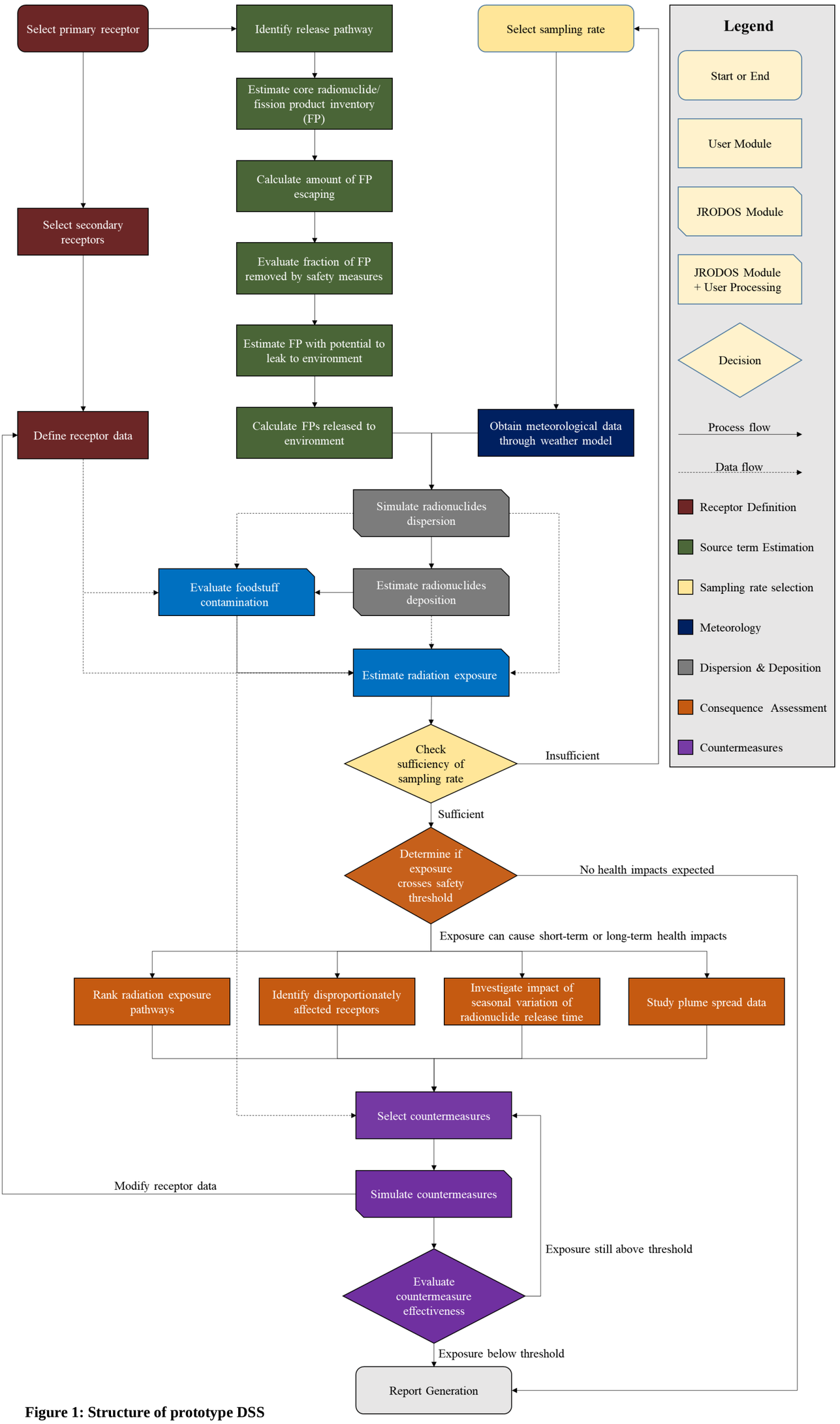

Figure 1: Structure of prototype DSS

2. IMPACT ASSESSMENT

This section aims to answer the first question from the objectives related to understanding the impact of accidents from multiple NPPs. This section describes the various modules used within the prototype DSS and discusses the results obtained from simulating accidents from multiple NPPs.

2.1. Methodology

As described earlier, the proposed prototype DSS consisted of several modules that work independently and pass the information from one module to the next for processing and are combined under one information framework. This approach is like the approach adopted by Lim et. al in designing the IMPAQT DSS (Lim et al., 2005). The complete DSS structure is shown in Figure 1, with the different modules explained below.

Many DSS's were created after Chernobyl to manage nuclear accidents. These DSS's include NARAC (USA) (Nasstrom et al., 2007), JRODOS (EU) (Ievdin et al., 2010), ARGOS (Worldwide) (ARGOS, 2014), SPEEDI (Japan) (Chino et al., 1993), and ONERS (India) (Raja Shekhar et al., 2020). These DSS's typically study the dispersion of radionuclides from the source, followed by deposition, food contamination, and human dosage at the end. For this study, modules from JRODOS were used for dispersion, deposition good contamination and dosage calculations due to its usage in many countries across the EU and Asia (Wengert, 2017).

JRODOS is a DSS developed by the EU after the Chernobyl disaster for addressing off-site emergency management after nuclear accidents. JRODOS is an integrated DSS that includes several simulation modules such as atmospheric & aquatic dispersion, atmospheric deposition, dosage estimation, and countermeasures testing. The system has been developed over three decades with the involvement of multiple institutions across the EU. It operates in more than 20 institutions across 16 nations in the EU and Asia at national and local levels (Ievdin et al., 2012; Wengert, 2017). The use of JRODOS across multiple countries lends confidence to its accuracy and versatility. The latter is especially important since Qatar (primary receptor) is a desert with a different climate to many other countries, as explained later. Furthermore, ARGOS and JRODOS share many common modules, which only increase the confidence in the use of JRODOS (Raskob et al., 2016).

In this study, the consequences were assessed qualitatively to suggest mitigation measures. It is expected that a fully functional DSS would quantitatively assess the consequence, simulate various mitigation measures and select the best mitigation scenarios based on user constraints. All of this would then be presented to the decision-maker in a standardized report format. Thus, using a DSS provides a logical framework to address the complexities and uncertainties of nuclear accidents. Furthermore, this approach is in line with FEMA's guideline to use a 'logical and analytical problem-solving process' (FEMA, 2010).

Currently, only the spread of radionuclides through the atmosphere was studied. Ideally, the DSS would also account for the hydrological dispersion of radionuclides within the Arabian Gulf, which is Qatar's primary drinking water source (Planning & Statistics Authority, 2017b). However, hydrological dispersion was not included due to the unavailability of requisite data on the Arabian Gulf.

2.1.1. Primary Receptor Selection & its Subdivision

The Middle East is witnessing exponential growth in nuclear power. This trend is can easily be seen in Figure 2 below. In particular, Iran, UAE, and KSA have spearheaded the development of NPPs within the region. In Figure 2, it can be seen that NPPs surround Qatar, with many of these closer to Qatar than to their home capitals. Thus, Qatar is an excellent case study to test the use of a receptor-centric framework. Consequently, Qatar was considered the primary receptor for this study.

Currently, only Barakah and Bushehr NPPs are operational. Thus, these were included in the study. Of the remaining planned NPPs, Umm Huwayd was included due to its proximity to Qatar when compared to Darkhovin and Makran Coast NPP and position relative to Qatar. Since Khor Duweihin is to the southeast of Qatar like Barakah, both plants are expected to have similar results upon simulation. On the other hand, Umm Huwayd is to the west of Qatar. Thus, simulating accidents from Umm Huwayd NPP would increase the diversity of the data and help illustrate the use of the frameworks

more clearly. All plants should be included in the future, and their impact simulated to obtain a more wholesome picture.

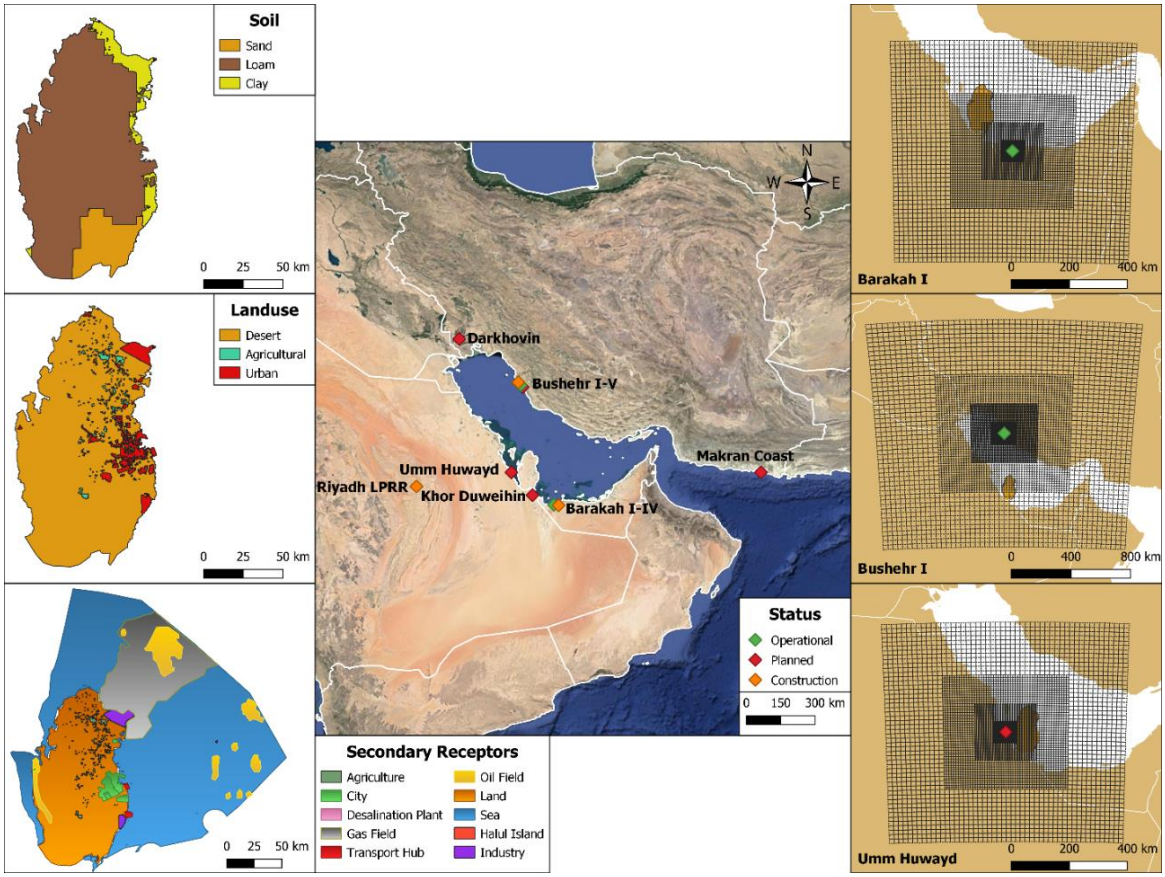

Figure 2*: Left (Top to Bottom):* Soil distribution, Land use Classifications, and Secondary Receptor Subdivision Maps.
***Middle*: Current & potential NPPs (Data from US EIA, NPR & World Nuclear Association (Johnson, 2018; Brumfiel, 2019; World Nuclear Association, 2020a))**
Locations are taken from Google Maps and satellite imagery
***Right*: Grid cells used for JRODOS calculations for selected NPPs**

The primary receptor Qatar was further subdivided into multiple secondary receptors. Areas of vital importance to the country, such as cities, transport hubs, industries, desalination plants, oil fields, and gas fields, were included as secondary receptors. The map of the secondary receptors within Qatar shown in Figure 2 above, while the list of secondary receptors can be found in Appendix A. The author's judgment based on the available population distribution and the anecdotal experience was used to select cities as secondary receptors. Inclusion of every small nonindustrial residential area was not feasible at this stage of the study. The only international airport (Hamad international airport) (Airport Technology) and the main seaport (Hamad Port) (Walker, 2016) were selected as transport hubs.

Qatar has three heavy industrial cities. However, only two were selected as secondary receptors. As the Dukhan oil field encompasses the Dukhan industrial city, the larger Dukhan oil field receptor boundary was used. Generally, when an area corresponded to two classifications, only one classification was assigned based on author judgment. Finally, Qatar also has a light industrial area within the city classified as a city due to the significant population on-site and nature of work performed (Shakespeare, 2014).

Similarly, Qatar has four major desalination plants. However, Ras Laffan industrial city encompasses the Ras Laffan desalination plant. Thus, Ras Laffan was classified as an industry, and only three desalination plants were included as secondary receptors. Special attention was paid to desalination plants as essentially all potable water

in Qatar is obtained from desalination (Mannan et al., 2019). In Figure 2, desalination plants are not visible due to their small size relative to the other receptors

As the hydrocarbon industry is the main contributor to Qatar's economy, oil fields and gas fields were also included (Planning & Statistics Authority, 2018). Fields on Qatar's mainland and exclusive economic zone (EEZ from (Al-Qaradawi et al., 2015)) were included (Al-Siddiqi and Dawe, 1998; "Qatar Blocks and Fields," 2014). Finally, Halul Island was given a unique secondary receptor classification as it serves as an army base, industrial site, and environmental protection site (Qatar Petroleum). Thus, vital infrastructural areas have been included in the analysis as recommended by FEMA (FEMA, 2010). All receptor boundaries were drawn using satellite imagery and district maps obtained from Google Maps as applicable.

Receptor Data

This section describes the receptor information gathered to adapt the simulations to Qatar and any preprocessing needed. Attempts were made to include data from as many diverse stakeholders as possible since FEMA recommends involving 'all stakeholders in the community' (FEMA, 2010). The information includes land use maps, soil distribution maps, population maps, food consumption habits, and inhalation rates. A detailed overview of the preprocessing performed and the assumptions used are discussed in Appendix A.

A combined land use/ soil classification map was obtained from Hassan et al. They combined data from the harmonized world soil database (HWSD) and a 2013 Qatari geological study with Google Earth satellite photos to obtain these maps. The soils were classified using reference soil groups of the world reference base for soil resources (WRB) (Hassan et al., 2020). These were reclassified into peaty, loamy, sandy, and clayey classifications to match JRODOS input. The maps were reclassified using the sand- clay-silt composition for the WRB soil types from the HWSD database and the USDA soil texture triangle (United States Department of Agriculture; FAO/IIASA/ISRIC/ISSCAS/JRC, 2012). Similarly, the land use map was reclassified as urban, agricultural, undefined grassland, and water. These maps are shown above in Figure 2.

Population distribution maps for 2017 were obtained from the Ministry of Public Health (Hassan et al., 2020). This year was chosen based on available data at the start of this project. The food consumption data was obtained from the Household Expenditure and Income Survey (HEIS) from 2013 (Ministry of Development Planning and Statistics, 2013) with meat consumption data from a study by Al-Thani et al. (Al-Thani et al., 2017b). No data from more recent years was available. The HEIS data was available as monthly household consumption rate for Qatari and Non-Qatari households separately. Thus, the HEIS data was converted into individual consumption rates using household size for both types of households. A weighted average based on the two population

subgroups was used to determine Qatar's representative individual consumption rate for different foods.

Only food grown within Qatar was only included in the calculation of the radiation dose through ingestion. It is expected that Qatar would only import food from countries unaffected by the nuclear accident. A similar approach was also followed by Poon et al. when estimating the radiation ingestion dose in Hong Kong, following a hypothetical nuclear accident at Guangdong NPP (Poon et al., 1997). However, it is to be noted that Qatar imports a significant amount of food from its neighbors (World Integrated Trade Solution). Some of them are also likely to be impacted by the same accident. A future avenue of work would be to include these countries in the simulations to understand Qatar's complete food supply chain better. Such an approach would give the country more tools to minimize disruption to the food supply chain. This approach would require a detailed breakdown of the origin of the imported food and significant receptor data on the neighboring countries.

Subsequently, the food consumption was scaled down using Qatar's agricultural production data obtained from the Planning Statistics Authority. This data included crops grown, animals reared, and agricultural yield (Planning & Statistics Authority, 2017a). For example, 16% of vegetables were produced locally; thus, food consumption of root, leafy, and other vegetables was scaled down to 16% of the individual consumption rate. All other pertinent assumptions and consumption rates used in this study are shown in Appendix A.

The average skin surface area was calculated to be 1.87 m^2 based on an estimation formula by Yu et al. as a function of height and weight (Yu et al., 2010). The height & weight data were taken from a Qatar Biobank report (Al-Thani et al., 2017a). The fraction of time spent indoors (occupancy rate) was estimated to be 90% based on EPA guidelines and recommendations by Andrade et al. in their review of indoor air quality for sports (U.S. Environmental Protection Agency, 1989; Andrade and Dominski, 2018). This assumption also is in line with the author's anecdotal observations of this factor within Qatar. Indeed, some factors, such as bathing frequency (assumed daily) and the fraction of skin covered by clothes (assumed 80%), were assumed based on anecdotal observations due to the lack of data.

Ideally, each type of receptor would have its own dataset as stakeholder characteristics can vary across receptors. This approach is essential in larger countries where secondary receptors have greater diversity among themselves. However, due to a lack of data, uniform food consumption rates, occupancy rate, bathing frequency, skin covered percentage, among other factors, were used for all receptors. Thus, another future direction of work is to estimate these factors for the various secondary receptors within the country to allow for a more tailored response for each receptor.

Experimental data on radionuclide transfer within a desert ecosystem was sparse and was not changed from the default values. These defaults are based on the HARMONE research project results, which were a part of the EU's OPERRA project. This project sought to improve the environmental modeling and human dose assessment

capabilities of JRODOS (NERIS, 2016). The default inhalation rate within JRODOS for the EU was adopted for Qatar as no significant difference in breathing rate is expected between the EU and Qatar. Another parameter of note is the resuspension factor used to estimate the resuspension dose. The resuspension factor is estimated as a function of time. The coefficients are estimated based on the Chernobyl accident and are chosen to avoid underestimating the dose (Müller et al., 2003). Any other factors not mentioned above were left as JRODOS default due to lack of data.

2.1.2. Source Term Estimation

Source term estimation is an essential part of studying the impact of any radiological disaster. Any inaccuracies and uncertainties in the source term significantly impact dispersion calculations and subsequent dosage estimations. However, to simplify the computations, many authors have modeled the release with a consistent release rate over the accident duration, sometimes with a limited number of radionuclides (Pirouzmand et al., 2015; Min and Kim, 2018; Liland et al., 2020). However, Mehboob et al. and Jafarikia et al. have shown that radionuclides are not immediately available for release but have a time dependency. Furthermore, the source terms depend on factors such as the reactor type, core inventory, operational reactor history, accident sequence (Mehboob et al., 2015; Jafarikia and Feghhi, 2018). Thus, it is essential to use source terms specific to the reactor in question to obtain accurate results. Consequently, this

study uses time-dependent source terms, which are matched the NPPs analyzed as much as possible.

As per the US Nuclear Regulatory Commission (NRC) 'NUREG 1228' Guidelines, to calculate a source term, the first step is to identify the release pathway. The release pathway is the route along which the radionuclides escape from the core to the atmosphere. For example, the radionuclides can escape through leaks in the suppression pool, bypassing primary containment catastrophic failure, isolation valve failure, or steam generator tube rupture. Once the release pathway is identified, the five-step process described below can be used to calculate the source term (McKenna and Glitter, 1988). These steps were also used for source term estimation in this study:

1. Fission products (FP)/ radionuclide inventory within the core
2. Amount of FPs escaping the core
3. The fraction of escaping FPs removed by passive (deposition on surfaces) as well as engineering safety features (spray systems)
4. Amount of available FPs with potential to leak to the atmosphere
5. Amount of FPs released to the atmosphere

As for the release pathway, the accident is assumed to be a loss of cooling accident (LOCA) as LOCA one of the most common scenarios studied in nuclear safety (Joyce, 2018). The FPs that escape the reactor core are then collected within the primary containment. After a 0.5 hour hold up, the FPs are released to the atmosphere due to either a catastrophic containment failure or an isolation valve failure (100% release). Both scenarios were taken from NUREG 1228 guidelines, with both scenarios treated as

identical by the guidelines (McKenna and Glitter, 1988). Ideally, multiple different accident scenarios would be simulated to obtain a more wholesome picture. However, as the study's main aim is to demonstrate a proposed framework in impact assessment and countermeasure selection, only one accident scenario per NPP was studied.

The estimation of FPs available in every step above is a complex and involved process and requires extensive knowledge of the reactor and the accident sequence. These calculations are outside the scope of this project. Instead, representative in-containment source terms (corresponds to step 4 above) from the works of Mehboob et al., and Jafarikia et al. were used. The reactors in question are described in more detail in Appendix B. Mehboob et al. estimated the core inventory for a generic two loop 1000 MWe pressurized water reactor (PWR) for LOCA. They used an in-house code validated against buildup and decay calculation code ORIGEN 2.1.

Similarly, Jafarikia et al. estimated the Bushehr plant's core inventory using the IRBURNS code, which uses Monte Carlo code MCNP and ORIGEN 2.1. The core inventory is used to estimate a time-dependent source, which first increases then decreases exponentially. In this case, the molten corium and debris after the accident is considered as the time-dependent source. Finally, transport equations coupled with various release fractions estimate the in-containment source term (Mehboob et al., 2015; Jafarikia and Feghhi, 2018).

No source term was located for the Barakah reactor or the APR-1400 model, possibly due to this model's limited usage. Only two NPPs in South Korea use this model

in addition to Barakah (KEPCO). Consequently, Mehboob et al.'s in-containment source term was used for Barakah as the Barakah reactor is also a two-loop PWR (UAE Federal Authority for Nuclear Regulation, 2012). This generic PWR source term was scaled up by the number of fuel assemblies assuming that the fuel assembly for the generic reactor and Barakah's reactor provide the same amount of power.

Jafarikia et al.'s source term was used for Bushehr and Umm Huwayd. As no information on the Umm Huwayd's planned reactor was available, any source term could be used for Umm Huwayd. The source term for Barakah was not used to increase the diversity within the data and enrich the data. As Umm Huwayd is in Barakah's opposite direction, use of Barakah's source term may introduce some common patterns in the data.

The in-containment source terms were then multiplied with release factors from NRC guidelines to estimate the environmental source-term (corresponds to step 5). Release factors corresponding to catastrophic release from containment following a 0.5-hour holdup were then used to estimate the environmental source term (McKenna and Glitter, 1988). The following assumptions were used based on NRC guidelines:

1. All of the equilibrium radioactive noble gas inventory should be assumed to be available for leakage from the reactor containment (McKenna and Glitter, 1988). No reduction factors to be applied to the noble gas inventory
    - This inventory should be estimated based on the maximum full power operation of the core.
2. The environmental iodine was split into its components, as shown below (Soffer et al., 1995).
    - Elemental Iodine: 91%
    - Particulate Iodine: 5%
    - Organic Iodine: 4%

The environmental source terms were divided into hourly intervals to reduce computational overhead and ease of input into the JRODOS system. The final source term used for the two NPPs is shown in Figure 3 below.

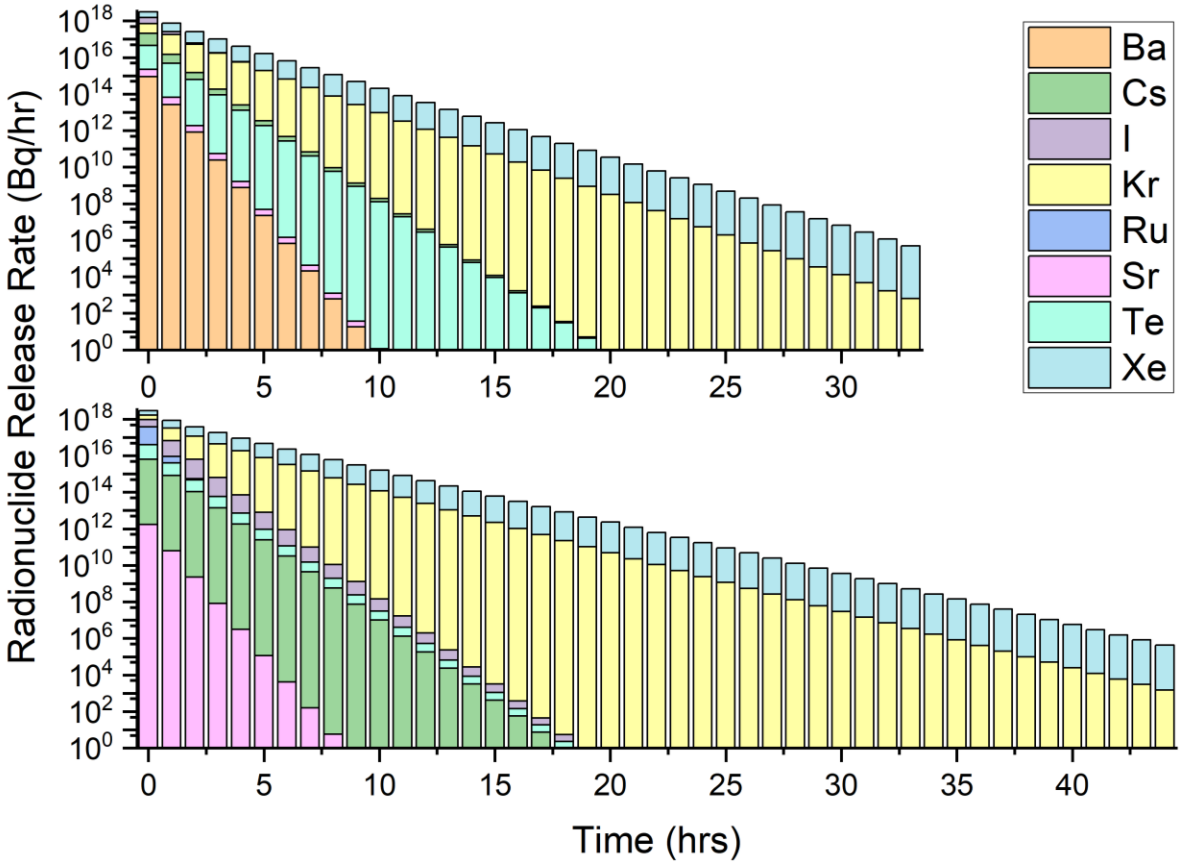

Figure 3: *Top*: Modified source term based on work by Mehboob et al. (Mehboob and Xinrong, 2012) used for Barakah NPP
***Bottom*: Modified source term based on work by Jafarikia et al. (Jafarikia and Feghhi, 2018) used for Bushehr and Umm Huwayd NPPs**

As seen in Figure 3 above, the releases last for 33 and 44 hours. The release was only modeled until the total release rate reached 1E6 Bq/hr. Based on the screening of the cloud dispersion, the release was not harmful to Qatar after this threshold due to the long

distance involved. This radioactivity level corresponds to 1 kg of low-level radioactive waste (World Nuclear Association, 2020c). The release height was arbitrarily chosen as 50 m for Bushehr and 70 m for Barakah based on each plant's maximum height containment dome (Emirates Nuclear Energy Corporation, 2018; Jafarikia and Feghhi, 2018). An intermediate height of 60 m was chosen for Umm Huwayd in the absence of any data.

2.1.3. Sampling Method

After calculating the source term, the release times need to be decided to obtain the relevant meteorological data and conduct subsequent calculations. The selection of release times is critical as weather fluctuations substantially impact the radioactive cloud spread and the subsequent impact on the receptor. Thus, any sampling technique to choose the accident release start time should be robust to account for these weather fluctuations. The main aim of sampling is to obtain a representative sample at a low computational cost. Such an approach would allow any user to simulate various accidents with diverse source terms being released from different NPPs for multiple years. The more diverse and complete the data is, the more power the decision-maker will have to arrive at the right decision. With this aim in mind, the sampling techniques used in previous studies on hypothetical nuclear accidents are described below. The sampling technique used within this study is described at the end.

Many studies relied on meteorological data to simulate the accident on days with the highest chance of a worst-case scenario. Some authors relied on wind roses alone

(Beeley and Kim, 2014; Pirouzmand et al., 2015). Others used wind rose data combined with precipitation patterns to select days with worst-case disaster potential ((Aliyu et al., 2014; Liland et al., 2020). Some others used the days with the highest precipitation and lowest temperature to decide the most likely day of the accident (Mohammed Saeed et al., 2020). As mentioned earlier, this approach can lead to response plans which create an unnecessarily high economic and social disruption as they do not account for accidents with relatively lower impacts. However, given that many authors relied on this method, the wind rose sampling approach was tested and compared to the results obtained from the stratified random sampling approach below in section 2.1.3.1.

Sohrabi et al. use cyclic sampling to choose the release time. Meteorological conditions that occur more frequently were assigned an equal probability and sampled (Sohrabi et al., 2013a). While an improvement over the previous method, this method tends to ignore 'black swan events', which are conditions that occur rarely but have potentially severe consequences (Taleb, 2007).

On the other hand, Dvorzhak et al. simulated 8760 accident cases by sampling release times hourly to fully account for the uncertainty in weather conditions (Dvorzhak et al., 2016). While promising, this method is very computationally intensive, potentially creates a significant amount of noise, and not suitable for all users. Thus, this method was not used as it is not in line with the primary aim described at the start of the section.

On the other hand, Min et al. simulate 365 accident scenarios assuming the release time as noon daily (Min and Kim, 2018). This method is a compromise between

accuracy and speed. This method is very similar to the 'stratified random sampling' (SRM) method. In SRM, the population is divided into multiple strata based on one or more variables, and one or more random independent sample is picked from each stratum (Powers, 2010; Hankin et al., 2019). Thus, the SRM method was used in this study. This simulation period (2017) was divided into 365 equal strata/segments (1 day). Accidents were then randomly sampled in each segment to create the whole dataset. The leak release start time for every segment was chosen randomly to create a more representative sample by reducing selection bias.

An important parameter in this method is the number of accidents simulated per strata (S) as it affects the data quality. An insufficient number of accidents simulated would lead to low statistical power and introduce unintended biases into the decision-making process. If a low accident sampling rate is used, it is expected that the samples created each time would tend to be statistically different from each other. If the sample is statistically different for every run of the algorithm, the sample is unlikely to reflect all the population characteristics but rather a part of it. Thus, a sufficient accident sampling rate would ensure that the samples created by the JRODOS randomizer algorithm each time are not statistically different from each other. The above criterion was used to choose S as no specific guidance was located to select samples from a population with unknown characteristics and an unknown distribution.

To this end, a qualitative decision method was proposed to select the accident sampling rate to ensure final sample datasets reflect the population to the greatest extent possible with the given sampling method and randomizer algorithm.

The difference between accident sampling rates is compared by running statistical tests on the effective one-year individual dose for every NPP analyzed. This parameter was used for comparison as it is the critical parameter of importance in this study for impact assessment. The sampling rate for each NPP was tested differently since each region has its weather patterns and is at differing distances from the primary receptor (Qatar) and will require different sampling rates.

The first step is to decide what type of tests can be used for the generated data. Nayak et. al and Marusteri et. al. have provided a handy guide that can be used to select the statistical tests. Since the distribution is unknown and the date-dosage pairing is unimportant, nonparametric tests for unpaired data such as the Mann Whitney U test (2 datasets) and the Kruskal Willis tests (>2 datasets) can be utilized. If the samples are statistically different via the Kruskal Willis test, multiple pairwise comparisons using the Dunn's test can be performed to see where the difference lies. The Bonferroni correction was used for the Dunn's test as its most commonly used correction in academic articles. A confidence level of 95% is used for all tests due to its widespread use. (Marusteri and Bacarea, 2009; Nayak and Hazra, 2011; Dinno, 2015). The exact methodology is visualized in Figure 4 below.

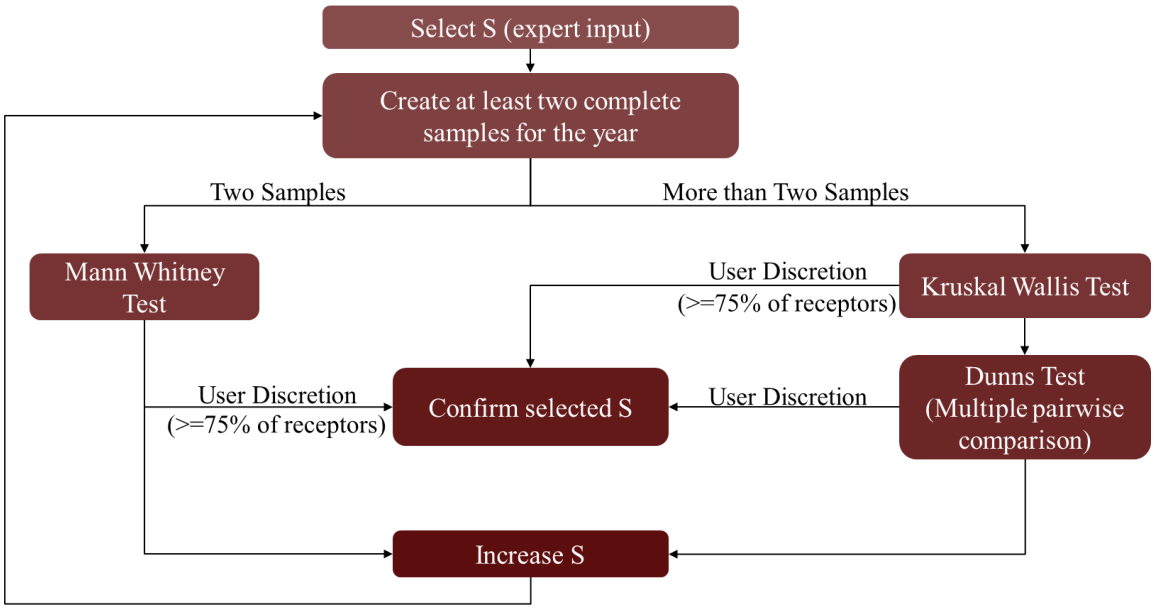

Figure 4: Qualitative decision method used to select the sampling rate

As shown in Figure 4 above, the first step is to obtain field expert input and select a sampling rate (number of accidents to simulate per day). Then at least two complete datasets with this rate are to be created, tested by three tests mentioned above. However, user discretion is to be used to analyze the results of the three tests proposed in Figure 4. For example, one might want all secondary receptors to have no statistical difference, while others may emphasize particular receptor types such as cities. For this study, a cutoff of 75% is used for Mann Whitney and Kruskal Wallis tests. If 75% of all secondary receptors show no statistically significant difference, then the sampling rate is accepted. For the Dunns test, users can analyze the pairwise comparison results and confirm the selected sampling rate based on the analysis. For example, 6 out of 7 samples tested show no

statistical difference. In such cases, the seventh is possibly an anomaly and can be ignored as per user discretion.

Two samples of rates S=1 and S=2 were tested with the Mann Whitney test to check the utility and robustness of the proposed methodology above. The results are shown in Table 1 below.

Table 1: Comparison of samples by Mann Whitney test for two sampling rates and all three NPPs

Percentage of receptors with no statistically different samples		
	S=1	**S=2**
Barakah	83%	22%
Bushehr	83%	52%
Umm Huwayd	65%	67%

Table 1 reveals interesting results. For single daily sampling (S=1), Barakah and Bushehr cross the stipulated 75% cutoff while Umm Huwayd does not. This result would imply that single sampling is sufficient Bushehr and Barakah, while higher sampling rates are needed for Umm Huwayd. However, on increasing the sampling rate, the number of receptors with no statistically significant difference drops for Barakah and Bushehr, while the result is essentially the same for Umm Huwayd. It is unclear why this behavior is seen.

One possible reason is the inefficiency of the JRODOS randomizer algorithm. It was suspected that either the randomizer algorithm failed to create a truly random set of accident start times or that the random sampling was not an equal probability sampling

but instead favored certain start times. To check both assertions, tests were done on the start hour of the accident as a time step of 60 minutes was used for the source term and dispersion calculations. Thus, the exact minute of release was not as important and accordingly not included in the randomness analysis. The Cox Stuart test, Bartels rank test, difference sign test, and Mann-Kendall test were performed to test the randomness and absence of possible trends. The null hypothesis of the first three tests was 'randomness of data', and the last test was 'no trend in data' (I.V and Lemeshko, 2014; Mateus and Caeiro, 2014). The tests were performed by combining all the release hours for the three NPPs for the S=1 sampling rate. Thus, a total of 1095 data points were tested. The results of these tests are shown in Table 2 below.

Table 2: Statistical Tests to Check Randomness of Starting Hour of Releases

Test	P-value
Cox Stuart	0.542
Bartels rank	0.1722
Difference sign	0.4547
Mann-Kendall	0.2697

From Table 2, all the tests have p-values above 0.05, so the null hypothesis cannot be rejected. These results mean the hypothesis of randomness and absence of a trend in data cannot be rejected. Thus, it can be concluded that the release hours created by the JRODOS algorithm are random, with no evidence to suggest otherwise. The next step

was to check whether JRODOS performs an equal probability sampling where the release is equally likely to happen at any hour of the entire day. Thus, a histogram of the frequency of release hours for S=1 sampling is shown in Figure 5 below.

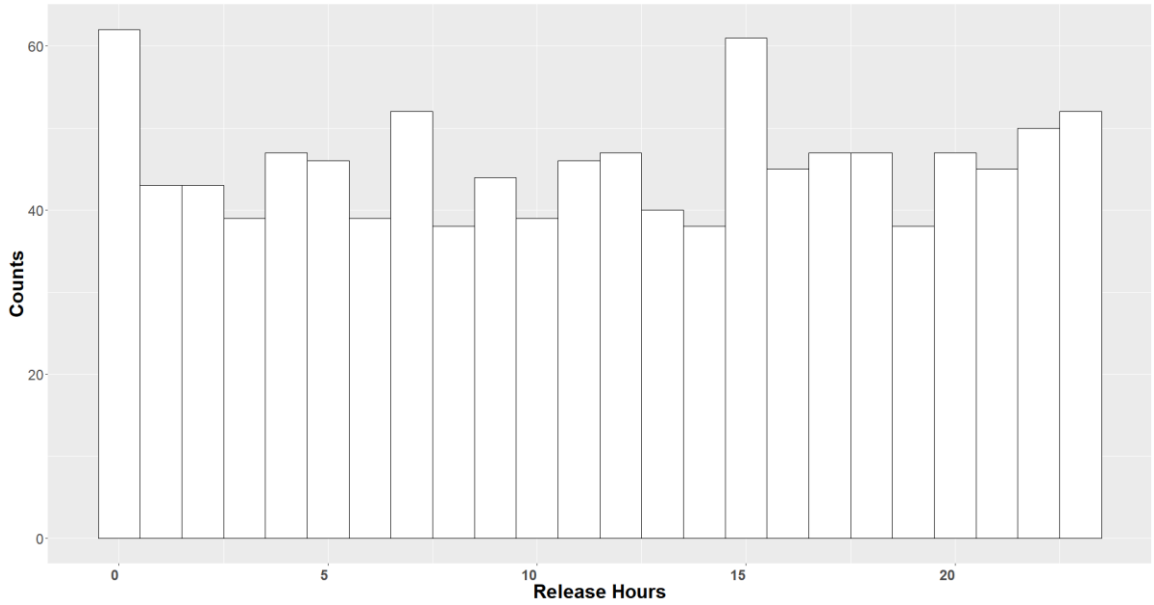

Figure 5: Frequency of Release Hours Picked by JRODOS for S=1 Sampling

From Figure 5, it can be seen that JRODOS sampling does not tend to be an equal probability sampling where all release hours are equally likely to be picked. Else a more uniform histogram across all three NPPs would have been seen in all three samples. The first and 15th hours were picked more often. A larger number of samples need to be tested to confirm this finding.

Thus, it is possible that samples created by S=1 sampling for Barakah and Bushehr were created for similar release times, which resulted in a high number of

receptors not having a difference. Alternatively, it is also possible that the methodology used to select the sampling rate need to be reformulated. Unfortunately, the current data is insufficient to make a clear judgment. More samples at the above-tested rates and higher rates (S>2) generated by JRODOS are needed for a conclusive judgment.

Due to computational limitations, only two samples were created for S=1 and S=2 rates. Consequently, the Kruskal Wallis branch could not be demonstrated in the current project and remains a future avenue of work. In this study, S=1 sampling was used as no other actionable result was obtained.

2.1.3.1. Wind Rose based Sampling

The wind rose for Bushehr NPP obtained from the NWP used is shown in Figure 6 below. The sampling was done based on the wind speed, wind directions and probabilities from the wind rose. Zero precipitation was assumed at Bushehr NPP as a more conservative estimate. The Pasquil stability classes were used (Pasquill, 1961). Strong insolation for daytime and thin overcast conditions for nighttime was assumed. The day's duration was set as 12 hours as an average between summertime (~14 hours) and wintertime (~10 hours) with sunrise at 6:30 AM (Time and Date AS).

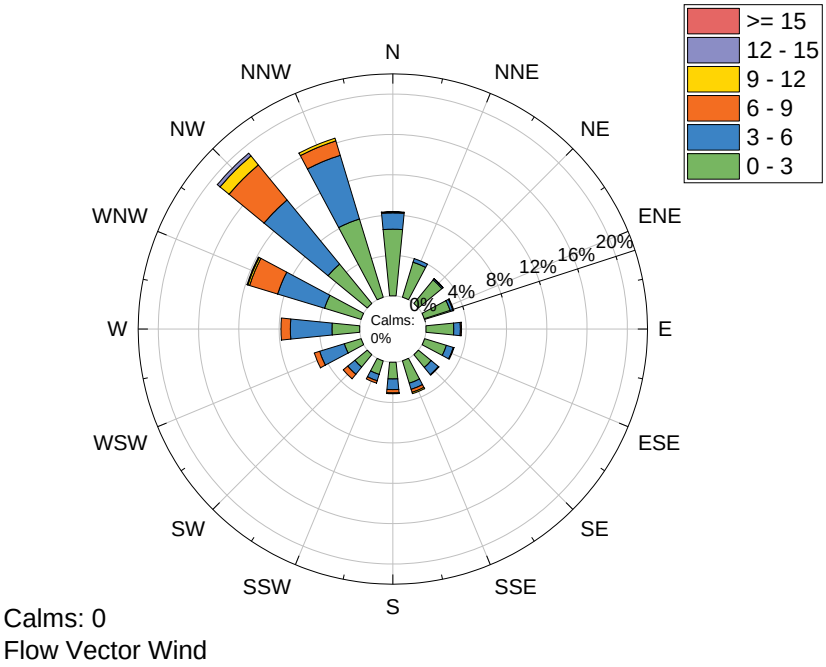

Figure 6: Wind rose showing direction and speed of wind in vicinity of Bushehr NPP

The distribution of effective radiation exposure at different secondary receptors is shown below in Figure 7. All doses above 0 mSv were visualized. In all subsequent boxplots, the upper and lower hinges of the boxes correspond to the 25th and 75th percentiles. The whiskers cover a range of 1.5 times the IQR from the hinges.

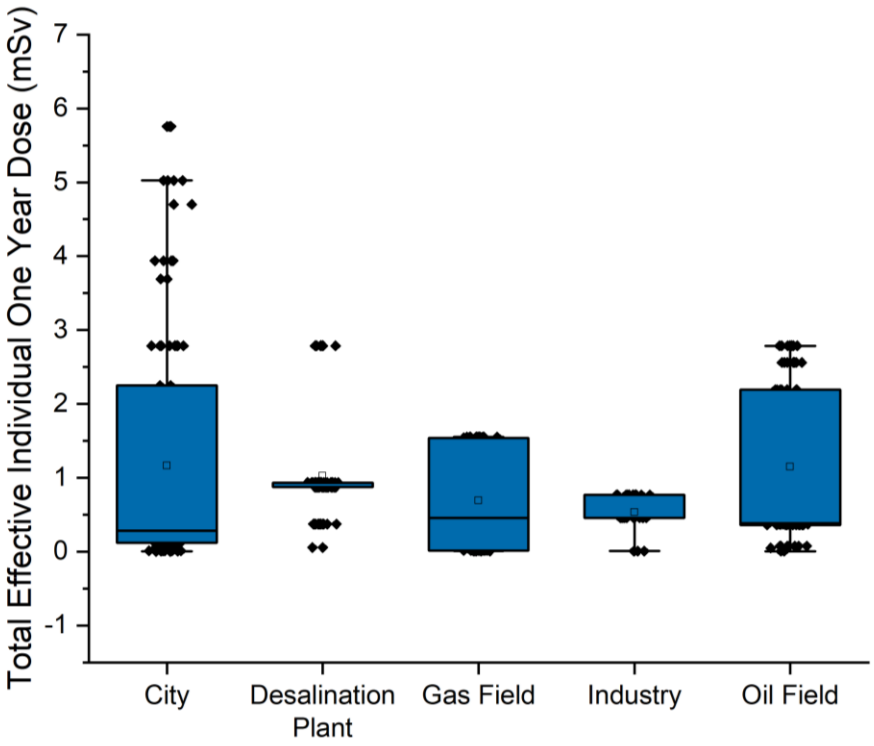

Figure 7: Effective one-year individual dose from release at Bushehr obtained from wind rose based sampling

Comparing Figure 7 above with Figure 8 below shows that using wind rose at the source for sampling significantly underestimates the dosage at far away receptors. In Figure 7, no combination of wind speed and wind direction leads to an effective dosage above the long-term damage threshold (50mSv). However, in Figure 8, the dosage even crosses the short-term risk threshold (1000 mSv). Furthermore, in Figure 7, not all secondary receptors are affected, which is also an erroneous conclusion. Thus, the wind rose approach is more appropriate for plant-centric studies where the focus is on the impact on the population living close to the NPP. However, this approach is insufficient

to study the radioactive cloud dispersion over long distances where there are significant changes in weather patterns. Thus, the sampling method adopted in this study is more appropriate for cloud dispersion over long distances.

2.1.4. Meteorological Model

Numerical weather predictions (NWP) from the NOMADS project of the US NOAA provided the required meteorological data for dispersion and deposition calculations. These NWP's include air temperature, wind speed & direction, rainfall characteristics, and sunshine coverage. In addition, these NWP's have global coverage, making it easier to simulate accidents from several sources for a primary receptor. The NWP with the finest grid size of 0.5° and smallest temporal resolution (update rate) of 3 hours was utilized (NOAA).

2.1.5. Atmospheric Dispersion & Deposition

JRODOS has three models for modeling the atmospheric dispersion; RIMPUFF, DIPCOT, and LASAT (Ievdin et al., 2019b). RIMPUFF is a Lagrangian mesoscale puff model that was designed to overcome the shortcomings of the Gaussian plume model. These shortcomings include the inability to handle inhomogeneous flows and turbulent flows (Thykier-Nielsen et al., 1999). DIPCOT is a Lagrangian particle model used to simulate the dispersion of pollutants over complex terrains in both homogenous and inhomogeneous conditions (Andronopoulos et al., 2002). Finally, LASAT is also a

Lagrangian particle model with a diagnostic wind field model present in the pre-processor to calculate dispersion when buildings are present. LASAT is recommended for use in systems with powerful computational capabilities (Raskob et al.). However, as the aim is to simulate a large number of cases (>1000) over a simple terrain (Refer to Figure 2), LASAT was not adopted.

Pasler-Sauer et al. conducted comparison and validation exercises between RIMPUFF and the DIPCOT model. They determined that both models show similar and realistic results under simple and moderately complex meteorological conditions. However, under complex conditions, DIPCOT has a better chance to obtain realistic results (Päsler-Sauer, 2010). Since Qatar and surrounding areas have a simple and relatively flat terrain (Refer to Figure 2), RIMPUFF was chosen as it performed faster compared to DIPCOT for the same case during initial testing.

A time-step of 60 minutes (vs. 10 or 30 minutes) was used as a compromise between computational speed and accuracy. The dispersion model was run for 72 hours for Barakah and 96 hours for Bushehr. Initial testing by trial and error showed minimal change in Qatar's total gamma dose rate after the periods mentioned above, respectively. The containment building height and width were also inputted as part of initial plume broadening calculations. The Bushehr reactor containment height and width were inputted as 54.50 m (Jafarikia and Feghhi, 2018). The Barakah reactor containment width was assumed to be the same as its height of 70 m (Emirates Nuclear Energy Corporation, 2018). In the absence of data, width and height of 60 m were used for Umm Huwayd.

The DEPOM model was then used to calculate the dry and wet depositions by utilizing RIMPUFF results (Ievdin et al., 2019b).

An adaptive grid was used for dispersion and deposition calculations. The grid is centered at the accident site. As such, the grid is finer at the accident site (NPP) and coarser as one moves away. The grid can be further divided into 1-5 rings of equal size cells as shown. The cells double in size as in every ring moving from inner to outer rings. The grids are characterized by the calculation radius, innermost cell size. JRODOS provides a limited number of grids based on pre-specified combinations of the calculation. The coarsest grid was utilized to allow for more extensive sampling.
A grid with a calculation radius of 800 km, the innermost cell size of 2 km, and five rings were used for Bushehr NPP. On the other hand, a grid with a calculation radius of 400 km, the innermost cell size of 1 km, and five rings were used for Barakah and Umm Huwayd NPP. The grids used can be seen above in Figure 2. However, these grids are significantly large compared to Qatar's size (160 km longitudinally & 80 km across (Crystal and Anthony, 2021)), which reduced the resolution of the receptor data. This issue and a possible solution are discussed in the Future Work section.

2.1.6. Foodstuff Contamination

The Terrestrial Food Chain and Dose Module (FDMT) module from JRODOS was used to calculate the food contamination and radiation exposure using the results from the RIMPUFF and DEPOM models results. FDMT only estimates the foodstuff

contamination only for crops grown. FDMT first estimates the contamination of plant products such as fruits, vegetables, hay, and wheat as a function of time. It calculates the contamination for plants used as human food as well as animal feed. FDMT considers contamination of the leaves, contamination due to root uptake, and resuspension. FDMT already has the required parameters such as weathering rate, translocation factors used for this calculation. It also requires a soil map of the simulation domain (refer to Figure 2) (Müller et al., 2003).

Next, the contamination of animal products such as milk, poultry, and eggs is calculated. The livestock exposure pathways considered here are inhalation of radionuclides and ingestion of contaminated feed. After this, factors for the radioactivity enrichment or dilution depending on the type of food processing and storage time are applied to estimate the level of contamination foodstuff (Müller et al., 2003). FDMT only calculates the maximum potential contamination. This calculation method was not considered a problem as the aim of foodstuff contamination calculation is to choose the foods to be targeted as part of agricultural countermeasures. As such, the relative difference in contamination between the foodstuffs is more significant than the absolute difference.

Of all the radionuclides, contamination by iodine (I), cesium (Cs), and their isotopes are of the highest concern (WHO and FAO, 2011). As such, foodstuff contamination by these two radionuclides was estimated. Two other radionuclides of lesser concern are strontium (Sr) and plutonium (Pu) which can be considered in future

work (WHO and FAO, 2011). However, it should be noted that the FDMT database lacks the requisite data (such as processing factors, translocation factor) to accurately estimate Pu contamination (Müller et al., 2003). Finally, for products that can be sold raw such as vegetables, fruits, meat, and milk, the raw dosage was calculated since the type of processing varies from facility to facility.

It is to be noted that FDMT calculates the food contamination assuming the food is grown in open-air farms. However, a significant portion of Qatar's food is grown in greenhouses (Burdon-Manley, 2017). The testing of Swiss berries after the Chernobyl accident showed greenhouses reduced the contamination in the food compared to foods from open-air farms. Specifically, strawberries grown in some greenhouses showed 95% lower contamination (2.7 Bq/kg radiocaesium) compared to raspberries, elderberries, and other berries grown outside (51±27 Bq/ kg) (Zehringer, 2016). However, relevant information such as the location and type of greenhouses was not available to determine the role of greenhouse location and type in contamination reduction. In fact, no comprehensive information on the reduction in contamination by the use of greenhouses was found.

This issue is further complicated because Qatari greenhouses utilize different designs than their counterparts in the USA or EU due to climate constraints (Karanisa et al., 2021). For example, greenhouses across the region use different cooling technologies such as positive pressure cooling systems with fans, negative pressure cooling systems & HVAC systems (Al-Mulla, 2006; Burdon-Manley, 2017; Alkhalidi et al., 2020). These

systems introduce a large influx of air into the greenhouses. The regular influx of air is expected to reduce the shielding effect of greenhouses by allowing easier access for radionuclides during an accident. Due to this uncertainty and general lack of data, contamination values obtained from FDMT were used without any post-processing.

2.1.7. Dosage Estimation

FDMT was used to calculate the radiation dosage to human beings according to the following exposure pathways (Müller et al., 2003):

- Inhalation – Cloud & Resuspended radionuclides
- Ingestion – Consumption of contaminated food (excluding drinking water)
- Cloudshine - Radiation from cloud
- Groundshine - Radiation from radionuclides deposited on different surfaces such as the ground, walls, and shrubs
- Skin – Radiation from radionuclides deposited on skin and clothes

FDMT calculates the inhalation dose from the radionuclides in the cloud and resuspended radionuclides separately. The former will be referred to as inhalation dose and the latter as resuspension dose in line with JRODOS convention.

An important assumption used within FDMT is assuming that the food is grown throughout the primary receptor at the point of consumption rather than the agricultural areas indicated in Figure 2 above (Müller et al., 2003). This assumption means FDMT calculates the food contamination for each grid cell separately based on the radionuclide concentration in the air and the deposition within that cell. The ingestion dose is then calculated based on these contamination estimations. This approach is problematic for

large countries with complex food chains where an urban area might be contaminated, but the farms supplying this area may not be contaminated. However, this assumption can be considered valid for Qatar due to its small size, simple internal food supply chain, and proximity of urban and agricultural areas. Due to Qatar's limited agriculture and simple food supply chain, it is expected that the ingestion dose should be similar across all receptors. This expectation can be used to test the appropriateness of the current assumption. Also, as a qualitative consequence assessment is used in this study, the exact level of food contamination and ingestion dose is not as important as the overall trends. Thus, FDMT was also used for estimating the ingestion dose.

Ingestion, groundshine, and resuspension dosages were estimated for integration times of 7 days, 30 days, 6 months, and 1 year. Longer integration times were not considered due to the uncertainty associated with the long-term modeling of any human behavior and subsequent dosage. The dosage for the remaining pathways is only associated with the deposition period, i.e., when the cloud passes over the receptor. The dosage for 11 organs and effective full-body dosage was also estimated. These organs include the thyroid, lungs, liver, uterus, colon, and marrow. All organ doses were calculated to understand the risk to the population better. Similarly, the final dose included dosage from all nuclides within the JRODOS database. Adult doses (>18 years) were only considered due to insufficient data for lower age groups. The doses were estimated for normal living exposure rather than worst-case potential exposure. The potential exposure is estimated by assuming the worst-case value for every parameter

(such as occupancy) to obtain the highest dose. This approach discards data about human behavior at the receptor, which is not in line with this study's objective. For the base case used for impact assessment, no mitigation measures were simulated.

The dosage formulas used within FDMT are linear. The RIMPUFF & DEPOM outputs, such as dry deposition and activity concentration near the ground, are multiplied with age-specific, organ-specific, and other such factors to obtain the dosage. These factors were compiled from various studies and guidelines from organizations such as the International Commission on Radiological Protection (Müller et al., 2003). However, some of these factors are 25-30 years old. Updating the dosage module with recent data (if any) is a future avenue of action. Nonetheless, the use of JRODOS across the EU lends confidence to the existing dosage models' accuracy.

The collective dose for the residential areas was also estimated in this study. Residential areas are defined as any receptor with a significant population within its boundaries, such as cities and industries. The collective dose is important as it incorporates the population distribution.

Each grid cell from the JRODOS simulation was assigned a population value based on the population distribution map. The 'Join attributes by location' option within QGIS was used for this operation to assign population values to cells that overlapped or intersected with a district from the population map. Due to JRODOS grid cells being larger than the population districts, some overlap occurred. This approach preserved the

spatial information of the results. The alternative was to use one population value for each city, which would overestimate the collective dose within each cell.

2.1.8. Consequence Assessment

The main aim of the consequence assessment module is to understand the impact of the disaster to deploy suitable countermeasures. Suitable countermeasures balance the expected public health gain against the possible cost and disruption as recommended by EURANOS for managing nuclear accidents in the EU. As the specific circumstances for the accident change from area to area, the consequence assessment structure and criteria change accordingly (Brown et al., 2007). So, in this study, different recommendations from the literature were used to conduct a semi-qualitative consequence assessment.

The first step is to determine the level of countermeasures (in terms of cost and disruption) justified by radiation exposure. For example, an accident expected to have detrimental health impacts in the short term would accordingly justify costly and disruptive measures. However, the same would not be justified for low probability long-term impacts. This judgment can be made by setting a threshold for acute (short-term) and long-term health impacts. The 1000 mSv threshold for acute radiation syndrome (ARS) can be used as the acute health impact threshold. The threshold for ARS is used because it causes serious health impacts such as radiation burns and nausea. Furthermore, it is likely to cause fatal cancers in 5% of all exposed people (WHO, 2016; World Nuclear Association, 2020c).

On the other hand, there is no agreement on the threshold to prevent the long-term consequences of radiation exposure, such as cancer and birth genetic defects. ICRP recommends keeping the lifetime dosage below 1 Sv. However, this guidance is challenging to implement given the significant uncertainty involved. Epidemiological studies on populations exposed to radiation suggest a significant increase in cancer incidences rate at doses above 100 mSv. At the same time, some other studies suggest a possible increase in cancer rate in the 50-100 mSv range (WHO, 2016; Vaiserman et al., 2018). In contrast, ICRP and US NRC use a 1 mSv/yr threshold under the controversial linear no-threshold (LNT) assumption (USNRC, 2018; Vaiserman et al., 2018). Since typical background radiation in North America can reach 3 mSv per year with an abdominal/pelvic CT scan alone, resulting in a 10 mSv dose, the 1 mSv dose was considered to be too conservative for this study (IAEA, 2016; World Nuclear Association, 2020c). Thus, the 50 mSv threshold was chosen for long-term cancer risk to balance the costs and potential benefits to the public.

The next step would be deciding the type of countermeasure to deploy for each receptor (such as agricultural, hydrological, medical). This choice is crucial to select the suitable countermeasure with the most significant benefit for the least cost. For example, if the ingestion dose is the highest, agricultural countermeasures will have to be adopted.

At the same time, attention needs to be paid to identify disproportionately impacted receptors as these would need extra resources. Especially if any critical infrastructure (such as desalination plants) is disproportionately impacted, more planning and resources

will be needed to ensure the continual operation of the facility. A useful metric that can be used here for cities is the collective dose that incorporates the population distribution and the individual dose. No similar metrics were found for other receptors and remains a future avenue of study.

The month in which the disaster occurs also has a significant impact on selecting and implementing countermeasures. Different weather conditions will require different approaches, such as rainy weather vs. snowy weather vs. summer. While Qatar does not have snow or significant rain, the summers can reach high temperatures of 50°C (Toumi, 2010), complicating mitigation measures such as evacuations and fire hosing external surfaces of buildings (Brown et al., 2007). Such high temperatures would make it difficult for workers in full PPE to enact urban countermeasures (refer to section 3.1 for urban countermeasures). Similarly, this information is useful when planning for special annual events such as pilgrimages and festivals. These events inherently have different characteristics such as increased attendance, special rituals, and restrictions requiring special measures.

Finally, the effectiveness of an excellent mitigation plan is significantly reduced if not implemented on time, as was the case with the Fukushima Daichi disaster (Funabashi and Kitazawa, 2012). Thus, an efficient early warning system needs to be in place to allow for the timely deployment of countermeasures. Therefore, the radioactive cloud spread data was qualitatively investigated to check whether the data could be used to guide early warning sensor placement. To this goal, the minimum arrival time of the radioactive

cloud for each accident from the different NPPs was estimated. The cloud arrival time was estimated at the EEZ boundary and the terrestrial boundary. The arrival time was measured at grid cells up to a distance of 0.01 degrees outward from either boundary. Furthermore, only one cloud arrival time was associated with one accident per day per NPP. Cloud arrival times were defined as the time elapsed between the start of release and any of the three following conditions being met. These conditions were chosen based on JRODOS recommendations (Ievdin et al., 2019a). However, these can be changed to suit needs such as sensor sensitivity.

- Time integrated air concentration (nuclide sum) near ground exceeds 1000 Bq*s/m^3
- Total cloud gamma dose rate exceeds 1nSv/h
- Total Ground contamination exceeds 100 Bq/m^2

The semi-qualitative method mentioned above can be summarized into the following concise guiding questions:

1. Are the expected radiation exposures higher than the threshold for either acute short-term or long-term harm?
    a. Is the one-year effective exposure higher than 50 mSv?
    b. Is the one-year effective exposure higher than 1000 mSv?
2. What are the critical exposure pathways of concern for each receptor?
3. Are any receptors disproportionately impacted?
    a. What is the individual & collective effective dose patterns for cities?
    b. Is critical infrastructure disproportionately impacted?

4. Is there a significant difference in the exposure depending on the month in which the accident occurred?
5. Can radioactive cloud spread data be used to guide the deployment of early warning systems?

2.2. Results and Discussion

The data obtained from the DSS has been used to answer the questions posed in section 2.1.8 above. All results have been obtained by filtering the data for dosages above 1 mSv below which no health effects are expected. The blue line represents the long-term threshold (50 mSv) and the red line the short-term threshold (1000 mSv) in the following boxplots. The use of boxplots helps overcome uncertainties associated with any single release as the aim is to obtain general trends within the data to drive countermeasures selection.

Furthermore, all probability density plots were created using kernel density estimation. Kernel density curves are smooth and better display the characteristics of the probability distribution. This method also uses the location of all sample points, revealing more information about the population from a finite data set (Weglarczyk, 2018).

2.2.1. Effective One-Year Individual Dose by Exposure Pathway

The effective individual dose received after a year through the various exposure pathways is visualized in Figure 8 below.

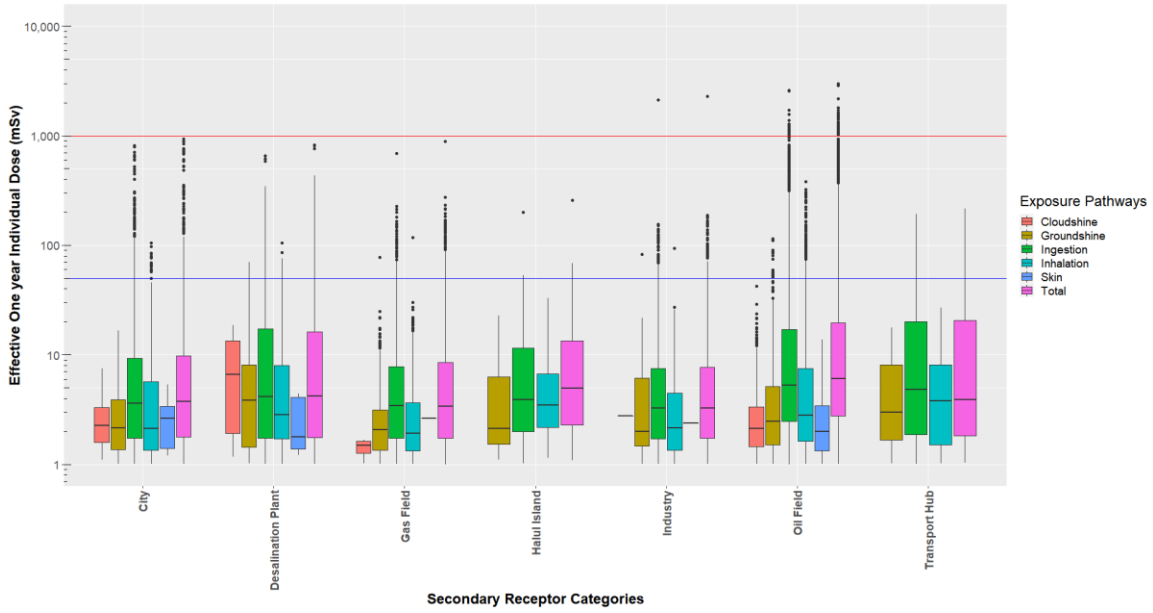

Figure 8: Effective individual dose received over a year for secondary receptor categories

In Figure 8, it can be seen that the expected radiation exposure is higher than the threshold for long-term health effects (50 mSv) for all receptors. In cities, desalination plants & gas fields, the dose approaches the acute ARS threshold (1000 mSv). However, the dose for oil fields crosses the ARS threshold and reaches 2974 mSv. Similarly, one case within the industrial receptor also crosses the ARS threshold 2294 mSv. Thus, there is a critical need for mitigation measures to protect the population with more severe mitigation measures to protect people working in oil fields.

In this case study, ingestion exposure is the critical contributor to individual doses for all secondary receptors. This result is most likely due to ingestion being a recurring source of radioactive dosage in the absence of countermeasures. Thus, the core part of

any mitigation strategy needs to target and significantly reduce the ingestion dose. The ingestion dose also shows greater uniformity (except oil fields) across the various receptors than other pathways. This result shows that calculating ingestion by estimating contamination at the point of consumption rather than growth is valid for small countries with simple food supply chains. The amount of radioactive contamination in different foodstuffs is explored later in the countermeasures section. The discussion regarding the disproportionate dose in oil fields & industries comes later in this section.

Inhalation is the second biggest contributor to the individual dose, while groundshine is the third most significant contributor. However, these doses seldomly cross 50 mSv. Thus, simpler, less disruptive measures to protect the population from non-ingestion doses can be used. The main focus should remain on mitigating the ingestion dose. The remaining two pathways (cloudshine and skin) vary in importance across the receptors. For most receptors, these pathways are not a critical source of radiation exposure. Cloudshine and skin exposure are negligible for transport hubs, cities, and industries with a more noticeable impact in other receptors such as desalination plants. For larger source terms with longer release times, these pathways may be of a greater concern due to longer cloud deposition times.

Furthermore, no resuspension dose can be seen in Figure 8, as the highest resuspension dose calculated was 0.016 mSv in the Dukhan oil field area. Thus, mitigation of resuspension dosage is not an essential part of the study for simulated

accidents. Any actions taken to control the inhalation dose from the radioactive cloud would likely suffice to mitigate the inhalation of resuspended particles.

Finally, from Figure 8, it seems that some infrastructures (oil fields and industries) are disproportionately impacted. All other receptors show dosage below 1000 Sv (the threshold for ARS) except oil fields and industries. Thus, the effective individual doses after one year across these receptors are shown below in Figure 9.

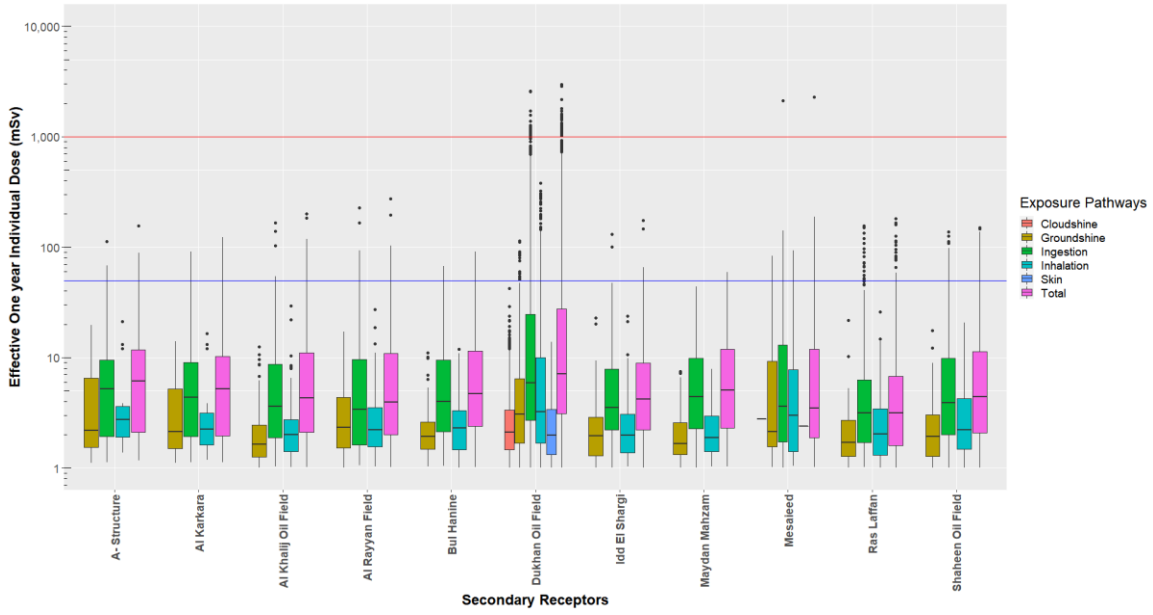

Figure 9: Effective individual dose received over a year for oil fields and industrial receptors

From Figure 9, it can be seen that only the Mesaieed industry and Dukhan oil field are disproportionately impacted. In both cases, all exposure pathways show a higher dose which means more resources are needed for mitigation in these receptors. Once again,

ingestion dose is the critical pathway of exposure. Here ingestion dose means the exposure through the food consumed by the people working in these areas. Two interesting and important results with regards to the ingestion dose need to be discussed. Firstly, while Dukhan & Mesaieed show a higher ingestion dose, these are further away from the agricultural areas. Thus, the FDMT assumption of calculating ingestion dose at point of consumption rather than growth due to proximity between agricultural and other receptors is less applicable. Thus, it is expected that both will have similar ingestion dose profiles as other receptors. In this case, these receptors will have a similar total dosage profile as other receptors and cannot be considered as disproportionately affected.

Interestingly, the remaining oil field receptors far from agricultural areas than Dukhan or Mesaieed show much lower ingestion dosage profiles (<227 mSv) than others. The FDMT assumption is particularly not applicable here and should be considered similar to nearby terrestrial receptors. Nonetheless, in this case, the error is not significant as the conclusion obtained from the qualitative analysis remains the same.

Finally, it should be noted that the sampling method used in this study is quite robust compared to the wind rose sampling approach as it identified cases with negligible, mild doses and severe doses. Finally, using a receptor-centric approach allowed the identification of receptors that could be disproportionately affected, ensuring everyone is protected. Thus, this section answers the first three questions posed in the consequence assessment section, which has provided significant guidance on the different mitigation measures to pick.

2.2.2. Individual vs. Collective Dose for Residential Areas

The individual and collective dose for residential areas is shown in Figure 10 below.

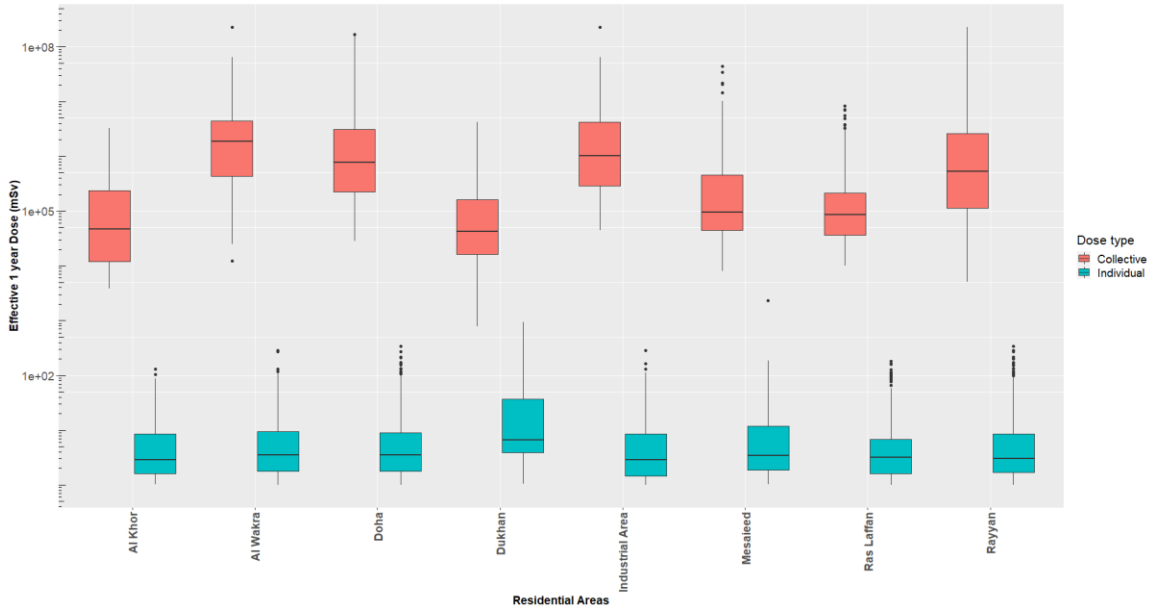

Figure 10: Effective one year individual & collective total dose for residential areas

Figure 10 illustrates how the distribution of dosage changes significantly between the individual and collective dose. While Dukhan tends to have the highest individual dose, it has a lower collective dose due to a lower population density than other cities. Other areas have similar individual doses but significantly different collective dose profiles due to the spatial variation in individual dosage and population distribution. Thus, from the above figure, the utility of using collective doses in allocating resources for emergency efforts can be easily seen. Furthermore, collective doses are particularly

useful for countries like Qatar, where large parts of the country are sparsely populated. As such, the use of collective doses would ensure resources are allocated proportionally to the population. Similarly, the collective dose calculation would be equally crucial in larger countries with more complex population distributions. A possibly novel use for collective doses is as cost functions to find optimal combinations of countermeasures to minimize the impact of radionuclide release. The author was unable to find similar metrics for other vital receptors. Thus, another avenue of study is to develop similar metrics for other receptors.

2.2.3. Variation of Dosage based on Accident Start Time

The probability distribution for individual dosage throughout Qatar's four seasons for all receptors combined is shown below in Figure 11. The dosages are shown in a log scale for the x-axis. For this case study, the seasons were defined as below:

- Summer – June to August
- Autumn – September to November
- Winter – December to February
- Spring – March to May

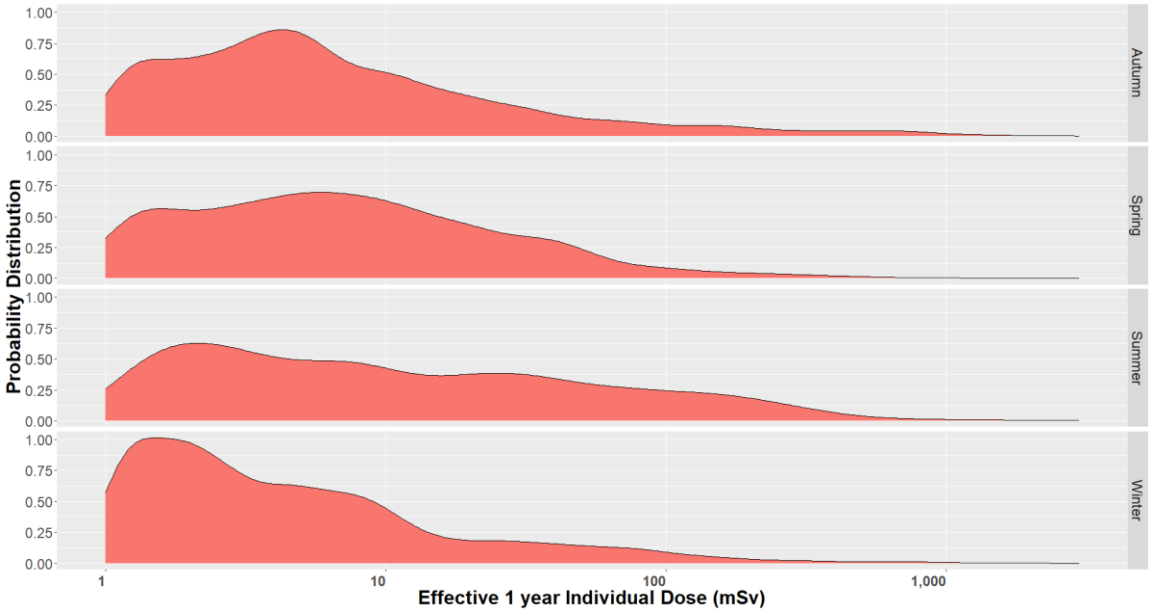

Figure 11: Seasonal distribution of effective one-year individual dose

In Figure 11 above, no particular variation is seen in the possible doses across the seasons, with all accidents having a slim but real possibility of crossing the 1000 mSv threshold. Accidents occurring in winter are more likely to have a lower dosage. Whereas accidents occurring in summer and autumn are more likely to result in a sizeable one-year dose than accidents initiated in other seasons. However, as accidents in all seasons are likely to cross 1000 mSv, emergency responders and the population must be prepared throughout the year.

2.2.4. Radioactive Cloud Spread Trajectory

The cloud arrival time for accidents from the three NPPs is shown below in Figure 12.

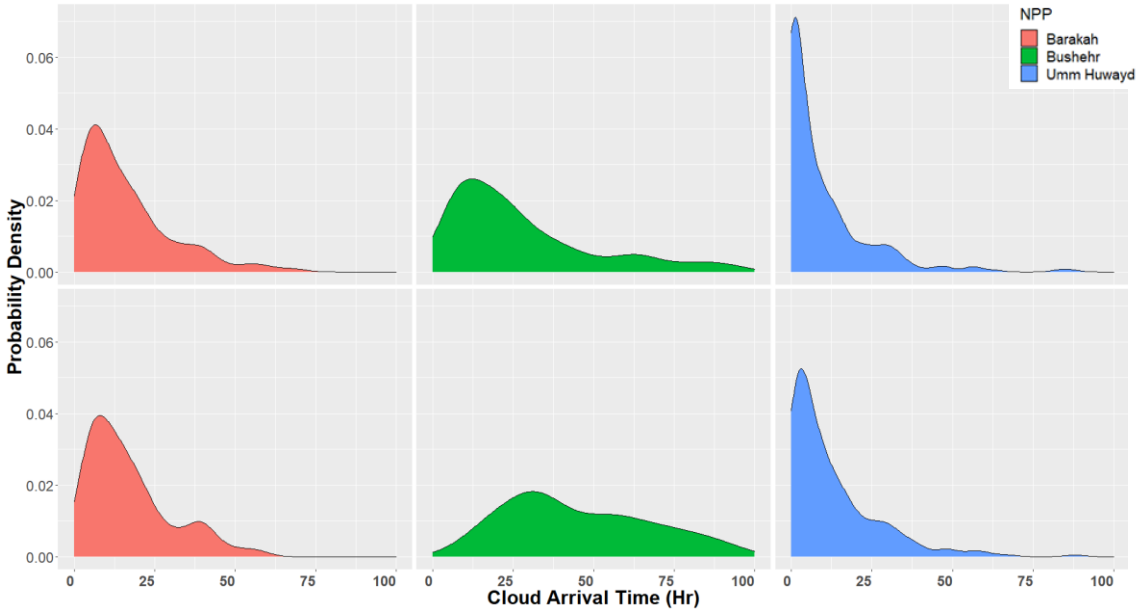

Figure 12: Cloud arrival time at the EEZ (Top row) and Terrestrial Borders (Bottom row) for accidents at the three NPPs

From Figure 12, it can be seen that the cloud arrival time varies from as little as one hour to 95 hours later. The cloud arrival time is linked to the distance of NPP from Qatar and the weather conditions. The arrival time for the closest NPP, Umm Huwayd, is the shortest, with the distribution biased to the first few hours. On the other hand, the arrival time tends to be longer for the farthest NPP, Bushehr. The longer arrival times are due to the weather conditions. A delay between the cloud reaching the EEZ border and the land borders can be noticed in Figure 12. This delay clouds crossing the EEZ and terrestrial boundary provides an opportunity to detect the cloud early for the Qatari mainland.

In many cases, the cloud initially moves away from Qatar and then shifts towards Qatar due to a change in wind direction. Similarly, all clouds that cross the EEZ border do not necessarily cross the land border, as shown in Table 10 below. Thus, it is recommended to implement early warning systems on the EEZ border in addition to the terrestrial borders to protect offshore workers. This result highlights the strength of a receptor-centric planning method. Such cases would require plans that focus on protecting the workers on offshore platforms rather than those on land.

Table 3: Percentage of Clouds that Cross Either EEZ or Terrestrial Border for accidents at the three NPPs

	EEZ Border (%)	**Terrestrial Border (%)**
Barakah	31	28
Bushehr	61	30
Umm Huwayd	78	71

Bushehr has a large percentage of clouds crossing the EEZ border but around half reaching land. This interesting result is due to the EEZ shape, which is wider, close to Bushehr, and narrower on the side of Barakah and Umm Huwayd NPPs. Since Barakah and Umm Huwayd are also closer to Qatar, any cloud that crosses the EEZ will likely cross the terrestrial border. However, leaks from Umm Huwayd are more than twice as likely to reach Qatar compared to releases from Barakah. Therefore, the vast majority of releases from Umm Huwayd have a significant impact on Qatar. It should also be noted,

not all clouds that reach Qatar have impacts that cross the long-term harm threshold. Many clouds may be significantly dispersed if there is a large gap between radionuclide leak and cloud arrival. Suggestion on early warning sensor placement is discussed in the future work section.

3. COUNTERMEASURE PLAN

A crucial outcome of any consequence assessment study is to choose countermeasures to deploy when an accident occurs. After the Chernobyl nuclear accident, many countermeasures were studied and implemented to mitigate the impact of the Chernobyl release (Kirichenko et al., 2012). The countermeasures were classified based on literature review as described below.

Emergency countermeasures primarily refer to mitigation measures implemented during the pre-deposition and emergency phase after detecting a radioactive cloud. These include closing windows and air ducts to reduce air flow, covering precious objects, sheltering, and evacuation. These countermeasures tend to be implemented immediately after detecting an accident. These methods protect the population by reducing their exposure to radionuclides in the environment but not directly targeting the contamination (Brown et al., 2007). Thus, these methods primarily reduce exposure through inhalation, cloudshine, groundshine, and skin exposure.

Agricultural countermeasures are countermeasures that reduce radioactive exposure from ingestion of contaminated food. This category includes short-term measures like food restriction and food processing and long-term measures such as physical and chemical treatment of soil (Segal, 1993). A significant amount of work has been done in this specific field. For example, Alexakhin and Segal independently identified and examined the effects of several agricultural countermeasures to mitigate

the impact of the Chernobyl disaster (Alexakhin, 1993; Segal, 1993). Yatsalo et. al created a DSS to assess and choose an agricultural countermeasure strategy to rehabilitate the land after the Chernobyl disaster (Yatsalo et al., 1997; Yatsalo, 2007). Similarly, Fesenko et. al retroactively studied the countermeasures applied in Chernobyl using the ReSCA tool (**R**emediation **S**trategies after the **C**hernobyl **A**ccident) to justify the countermeasures applied (Fesenko et al., 2010). Likewise, JRODOS & ARGOS have also created a module, AgriCP, for reviewing the impact of agricultural countermeasures after a nuclear accident (Gering et al., 2010). Shinano studied reducing contamination in food grown from farmlands surrounding the Fukushima Daichi plant (Shinano, 2016). Interested readers can find more information from the joint IAEA/FAO technical workshop held on the same topic (IAEA and FAO, 2020).

Hydrological countermeasures are countermeasures that reduce radiation exposure from ingestion of contaminated water or marine fauna. This category includes methods such as water restriction, blending of contaminated & freshwater supplies, wetland liming, and use of activated charcoal in water treatment plants. Interested readers can find more detailed information in the review by Smith et. al on methods to reduce the radiation contamination in water supplies following a nuclear accident (Smith et al., 2001). These countermeasures were not considered as hydrological dispersion of radionuclides was not conducted in this study.

Urban countermeasures are countermeasures that reduce contamination on surfaces such as walls, pavement, trees, and shrubs. Thus, they primarily target

groundshine exposure and reduce exposure through the skin and inhalation of resuspended radionuclides. Some examples include fire hosing surfaces, sandblasting surfaces, deep plowing, topsoil removal, and tree/shrub pruning. While these methods directly address the contamination issue, they also have several disadvantages. These create waste and can negatively impact the environment. Second, these methods can potentially be very disruptive and expensive. EURANOS has an excellent guide to urban countermeasures, albeit focused on Europe, which can be adopted modified for other countries (Brown et al., 2007).

Finally, **medical countermeasures** aim to reduce effective radiation exposure by using drugs such as prophylactics and other medical procedures. These can be used before expected exposure or even after the person is exposed. The most popular medical countermeasure used is Potassium Iodine which protects the thyroid gland from I-131. Some other examples (with their use) are calcium gluconate (Sr-90, Ra-226), sodium bicarbonate (U-235), Prussian blue (Cs-137, TI-201), melatonin (general), and genistein (general). Other methods include gastric lavage and stem cell transplantation. Interested readers can read more in the review by (Arora et al., 2010). Based on the results from the previous section, the relevant countermeasure strategy was chosen, as discussed below.

3.1. Methodology

The countermeasures are chosen to minimize the effective individual 1-year dose while also minimizing the economic and social disruption to society. Thus, not all

countermeasures are appropriate for Qatar. Evacuation within the country is not feasible due to Qatar's small size and arid topography. At the same time, evacuation to KSA is a drastic endeavor with many challenges. As this study aims to pick countermeasures with a high benefit to cost ratio, such drastic measures were not initially considered. If other countermeasures are determined to be insufficient, then more drastic measures can be considered. An easier countermeasure to implement is sheltering. Typically sheltering is considered as a complex countermeasure (Brown et al., 2007). However, the significant experience with COVID19 lockdowns has made it easier to implement a successful sheltering policy (FT Visual & Data Journalism Team, 2021).

Figure 8 also shows that the ingestion pathway is the critical pathway of concern for the current case study. Thus, agricultural countermeasures will form the core part of any protective strategy. However, many of these countermeasures, such as plowing and liming soil & crop rotations, were formulated for open fields and not greenhouses. At the same time, the data on the greenhouses within Qatar is inadequate. Thus, it is difficult to simulate the impact of open-field agricultural countermeasures on greenhouses due to lack of data. Consequently, only food restrictions were explored in this study. Since Qatar imports most of its food (Planning & Statistics Authority, 2017a), food restrictions should be viable. Qatar has a simplistic food supply chain, and a uniform ingestion dose reduction plan can be used across all receptors. However, a uniform mitigation plan for the ingestion dose may not apply to larger countries as there is expected to be complex

food supply chains and significant variability in food consumption rates. Thus, depending on the food source and receptor, a more tailored plan can be created.

Similarly, as discussed above, groundshine exposure was not considered to be a significant exposure pathway. Thus, no urban countermeasures were implemented to reduce economic and social disruption. Urban countermeasures can be included in future strategies if the current strategy is determined to be inadequate. Finally, as no data was collected on specific radionuclide dosage, medical countermeasures were not considered.

The countermeasure simulations are conducted by changing the receptor data parameter and running JRODOS similar to the methodology in Section 2. A more detailed description of how the countermeasures were implemented and the parameter changes are described below.

3.1.1. Sheltering

The first question is deciding the type of lockdown, from a mild lockdown to a curfew. Keeping with the aim of this study, a mild sheltering policy was envisioned in this study, similar to the COVID19 lockdown implemented in 2021 (Al Jazeera, 2021). In this study, a mild lockdown was arbitrarily defined as reducing all outdoor exposure by 50%. Thus, the sheltering policy was simulated in JRODOS by increasing the occupancy rate from 90% to 95%. In actuality, the government would need to carry out a cost-benefit analysis to decide which outdoor activities to restrict and accordingly define the occupancy rate.

The next question is the duration of the sheltering policy to be implemented. The duration can be decided by looking at the dosage profile. The lockdown should be implemented for the duration which results in the largest non-ingestion dose to the population. Thus, the variation of the non-ingestion, ingestion, and total dose with integration time for all secondary receptors is illustrated below in Figure 13.

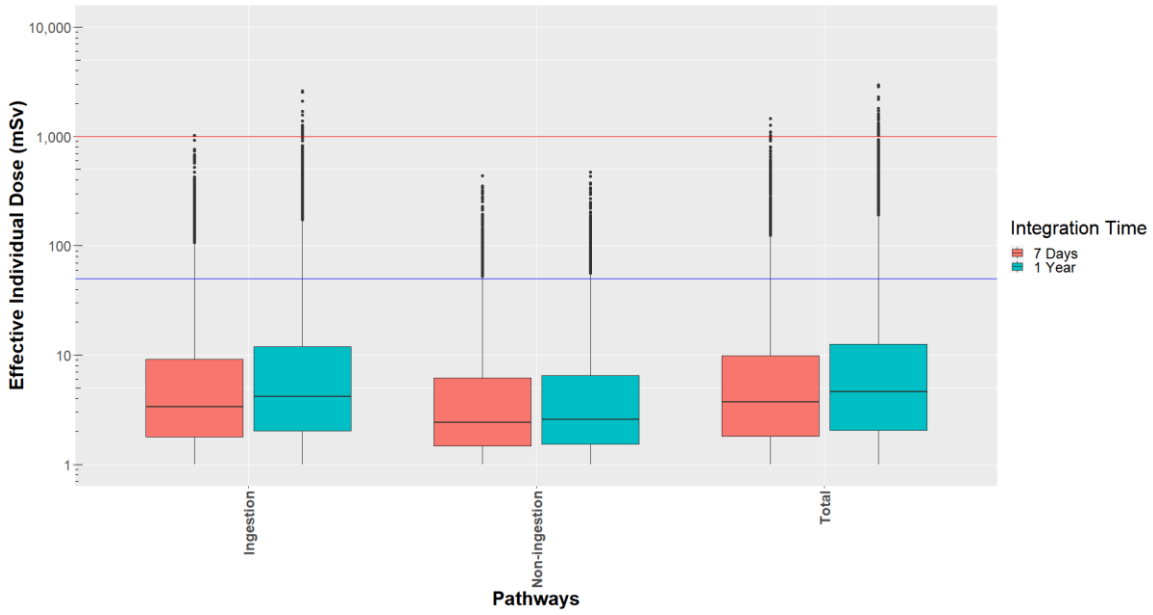

Figure 13: Radiation exposure by various pathways seven days and one year after the accident

From Figure 13, it can be seen that nearly all of the non-ingestion radiation exposure occurs in the first seven days, with contaminated foods ingestion driving the radiation exposure for the remaining days. Thus, sheltering should be implemented for seven days, and the duration can be increased as a safety margin depending on prevailing local circumstances.

However, the countermeasure simulation method used in this study calculates the one-year non-ingestion dose with one occupancy rate. Since nearly all of the dose is received within the first weeks, the calculated dose after one week of lockdown is expected to be very similar to one week of lockdown. JRODOS has an emergency countermeasures module, ‘ERMIN’, which can also be used. However, the ERMIN module data output did not match the information framework used in the current iteration of the prototype DSS. The use of the ERMIN module remains a future avenue of work.

3.1.2. Food Restrictions

It is essential to know which foods to restrict and the restriction duration before implementing food restrictions. A cost-benefit analysis is used to choose the former. This study aims to restrict just enough foods (without restricting all foods if possible) to drop the exposure below the exposure thresholds discussed earlier. A methodology for this is explored in this study. The restriction duration is equal to the decontamination duration. As decontamination of greenhouses is not explored in this study, the restriction duration was not studied.

The lack of the duration value will not affect the countermeasure simulation. The ingestion dose is calculated using only the consumption rate for each food, similar to the sheltering case. Therefore, the consumption rate of foods to be restricted will be set to zero. This approach practically means that either the food is wholly restricted for one

year or grown in Qatar's contamination-free areas before the end of the year. In either case, the radiation exposure is expected to be negligible from such food.

The guideline level (GL) for food contamination after a nuclear accident proposed by the Joint FAO/WHO Codex Alimentarius Commission was used to guide food restrictions. It is the maximum level of allowable contamination in food, above which governments need to decide whether to allow this food in their territory. The typical formulation of GL levels is shown in Eq. 1 below (IAEA, 2016).

$$GL = \frac{E}{M \times e_{ing} \times F} \qquad \textbf{Eq. 1}$$

Where GL is the guideline level (Bq/kg)

E is the allowable annual effective individual dose (mSv)

M is the age-dependent food consumption rate (kg)

e_{ing} is the age-dependent ingestion dose coefficient (mSv/Bq)

F is the contamination fraction

For GL calculation, the E was set at one mSv based on IAEA recommendation (IAEA, 2016). ICRP ingestion dose coefficients were used for e_{ing} (Eckerman et al., 2013). The sum of the contaminable food consumption data from Appendix C was used. The contamination fraction was set at one since the food consumption data inherently accounts for F. Finally, the lowest guideline values for I and Cs isotopes each were selected for a conservative estimate. Thus, the GL for I & Cs was estimated at 681 Bq/ kg and 788 Bq/kg, respectively. The calculated food contamination levels have been plotted

with the GL levels below in Figure 14 below. In Figure 14 below, only the GL level of 681 Bq/ kg is visualized to prevent cluttering. Since the two GLs are very close, Figure 14 shows the smaller 681 Bq/kg GL for visual clarity.

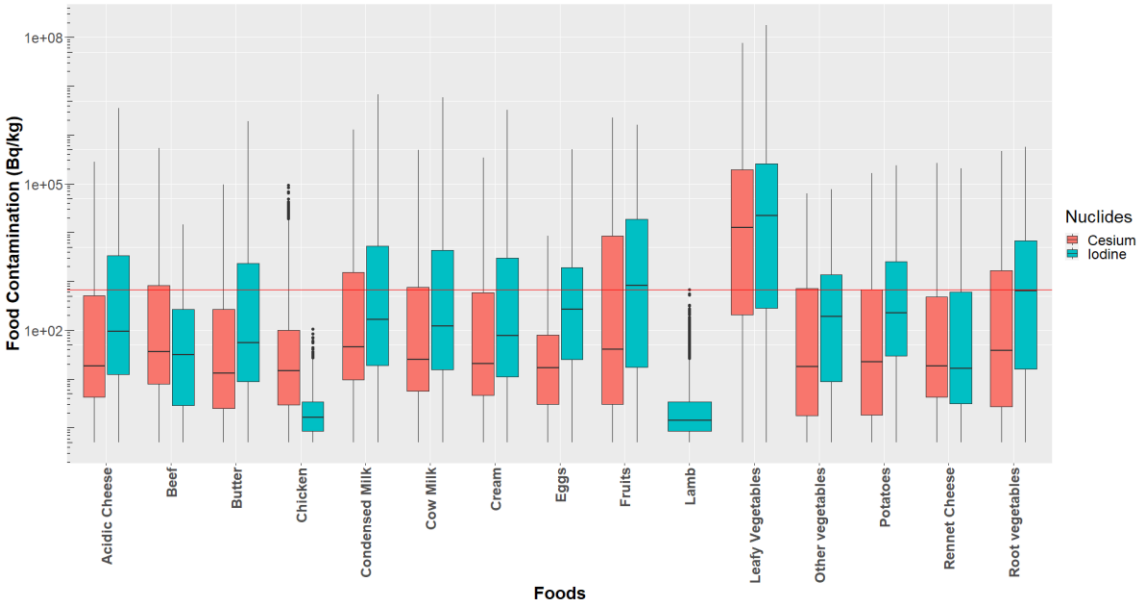

Figure 14: Iodine and cesium contamination of foodstuffs with guideline levels

From Figure 14, it can be seen that nearly all foods cross the GL. Leafy vegetables especially show disproportionately high contamination levels, likely due to their larger surface area compared to other foods. In contrast, lamb and chicken do not show high contamination levels (FDMT could not calculate cesium contamination of lamb, but it is expected to give similar results). It is not desirable to restrict all the foods except lamb and chicken as it would cause considerable disruptions. Thus, another method was needed to visualize the contamination data while accounting for GL to aid decision-making. Thus, the GL was normalized with the contamination data (CL) as in

Eq. 2 below to create a single 'food restriction metric' (FRM) from which one can easily visualize which foods to restrict. Foods with high FRM value should be restricted.

$$FRM = \frac{GL}{CL} \qquad \textbf{Eq. 2}$$

In this study, the median contamination level for each food was used as the CL. Alternatively, contamination values at higher percentiles or even the maximum contamination could be used based on user discretion. The FRM ranking is visualized in Figure 15 below.

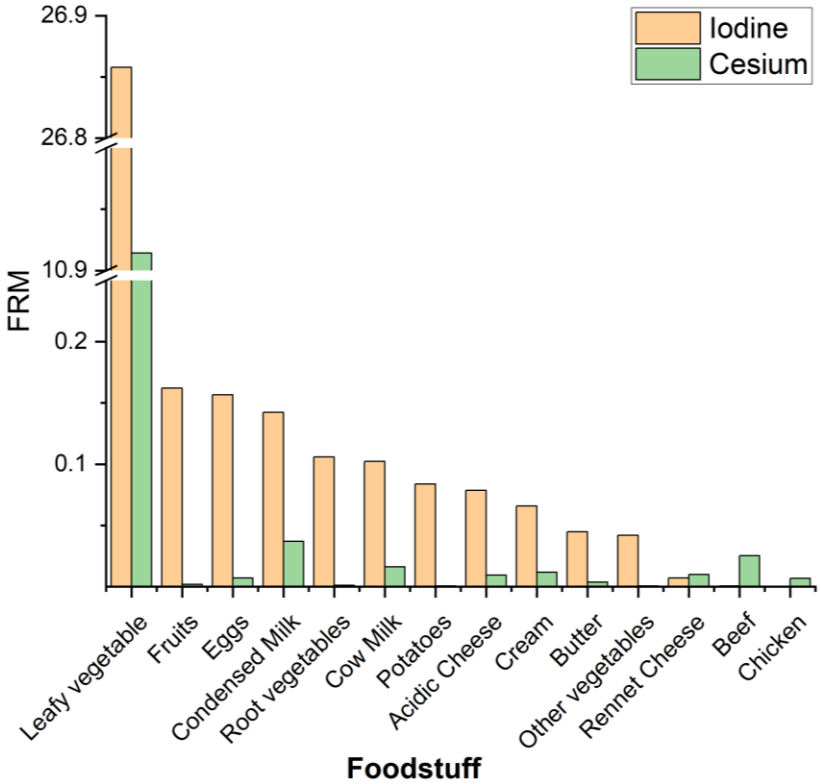

Figure 15: Lumped food restriction metric (FRM) for I and Cs radionuclides.

From Figure 15, it can be seen that iodine contamination is much higher than cesium contamination. Thus, it was decided to restrict three foods with the highest Iodine

FRM and three foods with high Cesium FRM apart from leafy vegetables. This decision is qualitative and can be improved by trial and error by simulating various countermeasures scenarios. Thus, leafy vegetables, fruits, eggs, condensed milk, beef, and cow milk were restricted in this case. So, 47% (in terms of daily food consumption rate) of the foods by weight considered in this study will be restricted.

3.2. Results and Discussions

The non-ingestion dose before & after sheltering is shown in Figure 16 below.

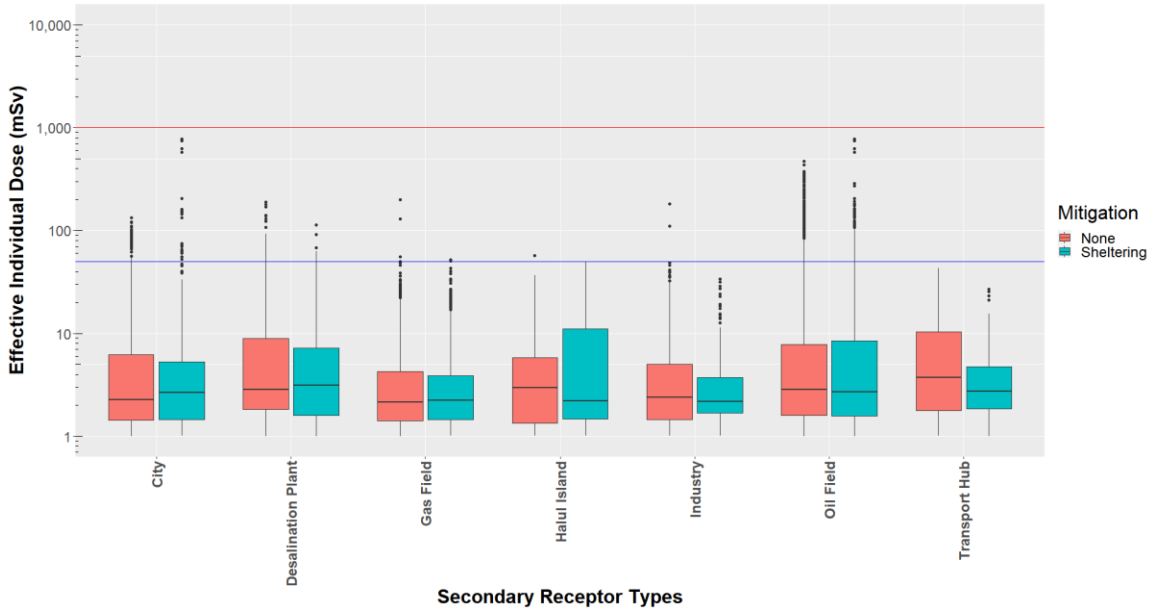

Figure 16: Non-ingestion Dose Before & After Sheltering

The results above seem to be anomalous, where the maximum dosage for receptors such as cities and oil fields increases after application of countermeasures. This

result is a direct consequence of an insufficient sampling rate. For countermeasure simulation, a new data set with an S=1 sampling rate was generated. Clearly, the new dataset has much higher dosage maximums which were not captured by the base case dataset is shown in Figure 8. Figure 17 below can be compared with Figure 8 to visualize this difference more clearly.

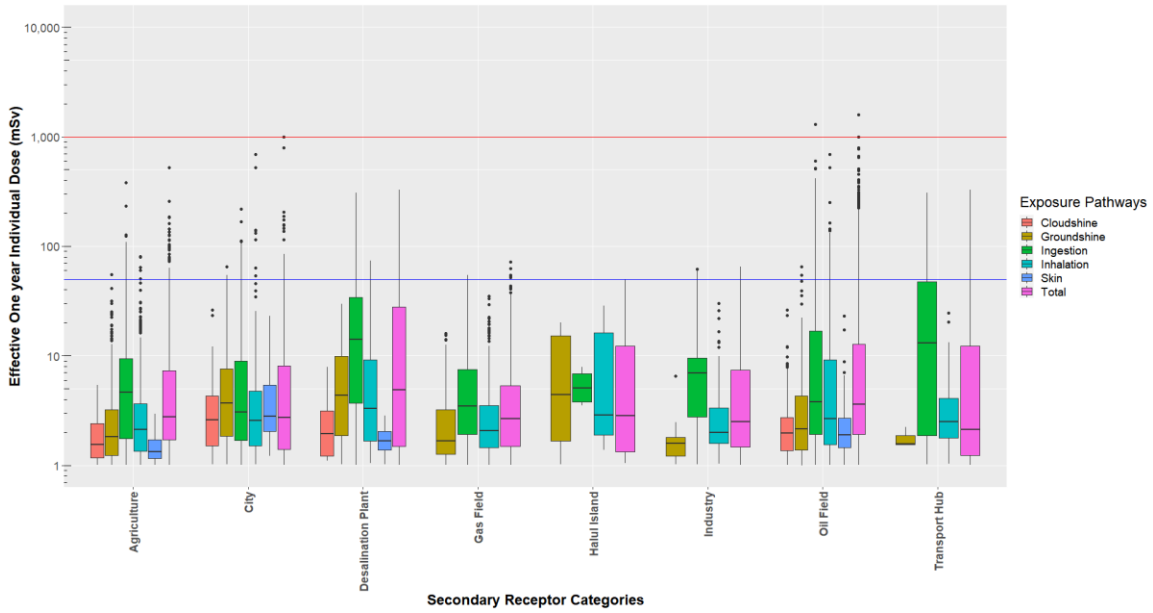

Figure 17: Effective individual dose received over a year with countermeasure deployment

Figure 17 above has significant differences with the bases case, such as the fact, inhalation has a much higher contribution across many receptors. There is a greater diversity among the dosage exposure pathways of different receptors. This diversity is most likely a result of the sampling rate capturing a more diverse set of accidents as well as the use of countermeasures. Thus, this figure affirms the urgent need for a robust

sampling method to capture mild, severe, and black swan accidents. Without such a sampling method, the conclusions drawn from the DSS will always be insufficient.

The effect of sampling rate makes it difficult to compare the base case and the sheltering countermeasure case. However, looking at the sheltering boxplots in Figure 16 alone, it can be concluded that either a stricter lockdown or more mitigation measures are needed to control the non-ingestion doses. Stricter measures are needed because the non-ingestion dose still is above the long-term harm threshold and even reaches the short-term threshold.

Similarly, the ingestion dose after application of food restrictions is shown in Figure 18 below.

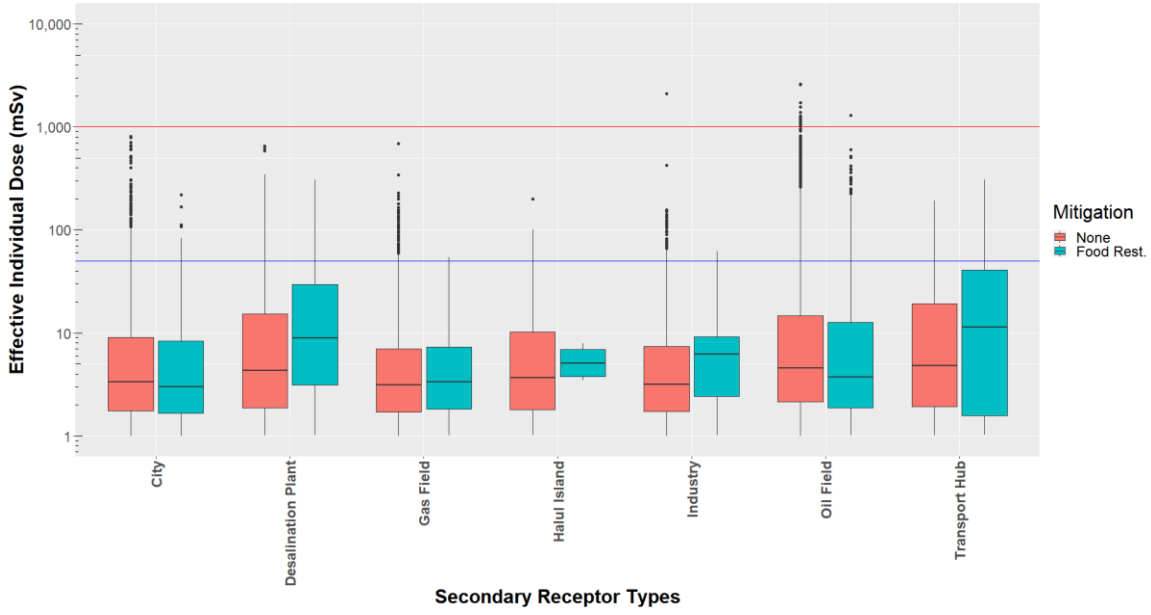

Figure 18: Ingestion Dose Before & After Food Restrictions

From Figure 18, it can be seen that the dose for the countermeasure simulation still crosses the long-term threshold. Thus, a larger number of foods need to be restricted to protect the population.

4. CONCLUSIONS

A prototype DSS for evaluating the impact of accidents from nuclear plants and selecting countermeasures was created. A novel receptor-centric framework for the DSS was proposed and utilized in line with FEMA guidelines. This framework was used to analyze the impact of non-simultaneous individual accidents in regions with multiple NPPs and obtain actionable insights to select a mitigation strategy.

Stratified random sampling (SRM) was used as part of the data-driven framework to consider a large number of accidents/hazards. SRM was shown to be superior to wind rose sampling for a release from Bushehr and its impact on Qatar. SRM allowed for identification for cases with negligible, mild, and severe consequences. A methodology to pick an optimal accident sampling rate within SRM was proposed. However, more data is still needed to accept or reject the utility of this method conclusively. The impact of an insufficient sampling rate on the quality of the results was also demonstrated.

JRODOS was used as a core part of this DSS. However, many aspects of the present JRODOS were incompatible with the receptor-centric and data-driven framework. These include grid type for exposure calculations, FDMT assumptions, and possible issues with the JRODOS randomizer algorithm. Possible solutions are discussed in the next section.

On testing the prototype DSS on Qatar for accidents from Barakah, Bushehr, and Umm Huwayd plants, the exposure from the accidents was found to cross both long-term and short-term exposure thresholds. The ingestion exposure was determined to be the critical pathway for exposure, followed by inhalation and groundshine. Cloudshine and

skin exposure were not of concern due to source terms with a small leak time/deposition period considered in this study. The resuspended radionuclides inhalation dose was determined to be negligible. The FDMT assumption of estimating food contamination and ingestion dose at the point of consumption rather than growth was determined to apply for Qatar. This assumption was valid mainly due to Qatar's small size and simple food supply chain. Mesaieed industry and the Dukhan oil field tend to be disproportionately affected, with more study needed to determine the ingestion dose for these receptors.

The utility of collective doses to identify areas requiring greater resources was demonstrated. Dukhan city was shown to have a higher individual dose but tended to have a much lower collective dose. No particular variation in total one-year dose with seasonal variation of release time was found for Qatar.

The radioactive cloud dispersion trajectories were found to have the potential to guide early warning sensor placement. In several cases, there is a significant delay between the arrival of cloud at EEZ border and terrestrial border, allowing for early warning for the Qatari mainland. Furthermore, the need for early warning sensors at the EEZ border to protect workers at offshore facilities was also highlighted. Many clouds that entered the EEZ region did not make landfall and enter the Qatari mainland. Suggestions for early warning system placements are also made in the next section.

Based on the consequence assessment, available data and resources, food restriction and sheltering countermeasures were selected. The sheltering was restricted to

7 days as nearly all the non-ingestion dose was received in the first week after the accident. Lamb and chicken were significantly less contaminated than other foods and did not need to be restricted. Normalizing guideline values with contamination levels (FRM) provided an easy and intuitive method to visualize foods to be restricted. An insufficient sampling rate made it challenging to compare the simulated base case and countermeasure case. However, from the simulations of the countermeasure case simulations, it was seen that the currently proposed strategy is inadequate, and a stricter strategy needs to be applied.

Finally, this project also highlighted the need for a fully functional DSS for Qatar to allow for an effective real-time response to an accident. Thus, countries need to invest and develop appropriate DSS with sufficient and accurate localization information to allow for a versatile response. As such, several avenues for future research were also identified throughout this project to develop a fully functional DSS adapted for the local region.

5. FUTURE WORK

Several avenues for future research were identified within this project. These avenues can be broadly classified into four categories. The most significant future research direction is completing the development of the DSS into a fully functional DSS. Furthermore, significant areas improvements in the modules used were also identified. Finally, the uncertainties in the data utilized for Qatar used also need to be addressed. Suggested strategies for placement of early warning sensors is also discussed below.

5.1. Further Development of DSS

The sampling rate is an essential cornerstone of the current DSS framework. Thus, more data needs to be generated to check the utility of the proposed method to select the sampling rate.

Similarly, a quantitative receptor-centric consequence assessment module needs to be developed. The module should sift through the large amount of data created similar to this study to give the user a complete picture of the consequences. This could be done using metrics to quantify the consequences at different receptors, such as food contamination guidelines and collective dose for cities. More such descriptive metrics with guide values should be developed to visualize the data intuitively, similar to the ‘Food restriction metric’.

Likewise, a quantitative countermeasure selection module is to be developed. Firstly, the module should pick countermeasures based on metrics such as economic cost, social disruption, FRM, similar to this study. The module then should suggest optimal

combinations of countermeasures by simulating their impact and using a decision-making algorithm. The metrics used for the consequence assessment section could be used as additional cost functions in this module to obtain optimal countermeasure combinations.

The hydrological modeling module also needs to be incorporated within the DSS to estimate the water contamination levels in the Arabian Gulf and contamination within the marine food chain. The POSEIDON model available within JRODOS is one possible model chain that can be utilized that can estimate both (Maderich et al., 2018). A significant amount of data on the Arabian Gulf also needs to be collected (from literature or experiments).

Furthermore, source terms unique to Barakah and other NPPs also need to be created. Similar studies should be conducted with the fully functional DSS for varied source terms, a greater number of NPPs and different release years to create an extensive accident database.

Finally, it is recommended that the DSS be programmed to run daily at set times to simulate accidents and generate data that allows for a speedy response. A similar approach as that of Bulgaria can be used. The Bulgarian DSS runs every 12 hours and creates a trajectory map of possible releases. Upon detection of an accident, another module is activated, producing radiation concentration and deposition maps to aid response (Syrakov et al., 2003).

5.2. Module Improvements

Many critical areas for improvement to the FDMT module used within JRODOS were identified, which need to be addressed if the FDMT module is to be used in the future within a receptor-centric framework.

The first issue identified was how JRODOS read the receptor data to calculate foodstuff contamination and dosage estimation. JRODOS used the RIMPUFF/DEPOM grid cells for reading the land use data, as shown in Figure 19 below.

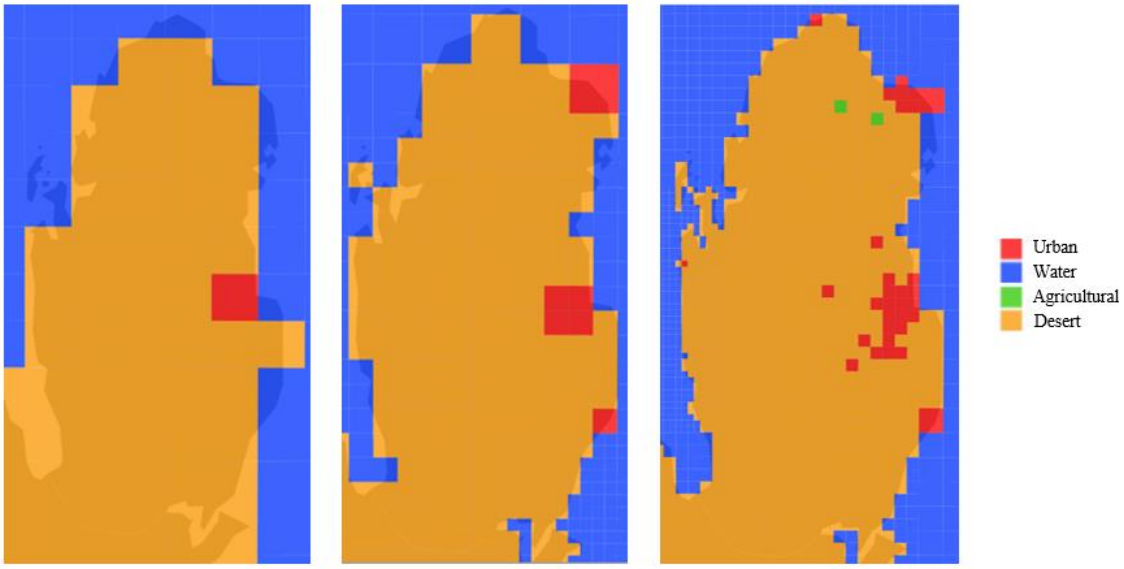

Figure 19: Land use maps used within JRODOS.
***Left to Right*: Bushehr, Barakah, Umm Huwayd**

It can be seen above that depending on the grid cell size and location of the NPP, JRODOS fails to capture nearly all of the spatial variations of the receptor data. In the

case of Bushehr, except Doha city, all other areas are considered to be a desert. This result is because the desert portion dominates in any given cell due to the smaller size of the urban and agricultural areas. Barakah and Umm Huwayd have the same problem, but Umm Huwayd captures more spatial variation in the land use data since it is closer to Qatar and uses a smaller grid size. As a result, a significant amount of the spatial receptor data (land use, soil use, and population distribution) is lost. While this approach is appropriate for a plant-centric study due to the finer grid at the source, this approach reduces the accuracy under a receptor-centric framework. Especially when the receptor is much further away from the NPP, as is the case for Bushehr. However, this approach had an unintended benefit for this project. The use of big grid cells reduced the error in foodstuff contamination, and ingestion dose calculations since the point of ingestion and consumption were covered by one grid cell due to their proximity and Qatar's size. For comparison, Figure 20 below shows how the land use map would look like the grid was centered on Qatar.

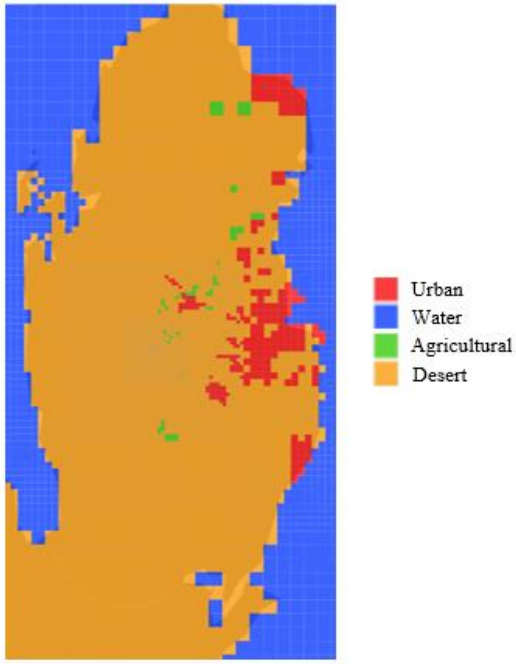

Figure 20: Land use maps used within JRODOS if the grid was centered on Qatar

Nearly all of the land use details are captured. A possible solution would be to use coarser grids for dispersion and deposition calculations but using finer grids for the receptor to capture the essential spatial variations. This option is currently unavailable in JRODOS as one grid type is currently used for all modules. It is hoped that future versions of JRODOS would incorporate this idea.

Secondly, an option to estimate the food contamination and ingestion dose based on agricultural areas rather than the point of consumption is needed. The user should be able to define the food grown in each agricultural area. This approach would significantly improve the accuracy of food contamination and ingestion dose calculations. Thus, models to estimate the contamination of complex food supply chains are needed. A possible solution is to calculate the ingestion dose from each food separately throughout

the primary receptor. However, the ingestion dose for the agricultural area growing that food would be kept and rest discarded. These ingestion doses can then be added to obtain one unified but representative ingestion.

Furthermore, studies are needed to determine the level of foodstuff contamination in greenhouses compared to open-air farms. Given the rapid increase in greenhouses use, especially in Qatar and across the region, this is an essential avenue of research.

Finally, the FDMT model requires more data to improve contamination and dosage predictions. For example, the current FDMT model lacks requisite data to estimate Pu contamination within foodstuffs. Similarly, the factors used for estimating the radiation dose to human beings are 25-30 years old and need to be updated. Thus, the data within FDMT used for estimating dosage needs to be improved.

5.3. Data Uncertainties

Continuous endeavors need to be made to update and refine receptor data to ensure accuracy. For example, the food consumption rates which were taken from a 2013 study are eight years old and should be updated soon and regularly. The data should be divided into subgroups to create unique data sets for each secondary receptor. Factors such as the occupancy rate and average skin coverage need to be estimated for Qatar. Regular stakeholder communication is essential to update and refine receptor data. Similarly, experimental data on radionuclide transfer within a desert ecosystem is another significant avenue for future research.

5.4. Design of an Early Warning System

Thus, one possible strategy for early detection is to place sea-based radiation measuring stations within Qatar's EEZ to create an early warning system. Another strategy is to create a land-based monitoring system similar to that of the EU. The EU stipulates a minimum areal density of 1 measuring station per 1000 km^2. Furthermore, for closer to NPPs, eight stations must be placed in a circle of diameter 2 km, with more stations if a larger diameter is chosen. Information is shared between all stations and allows for quick response to disasters (Dombrowski et al., 2017). A combination of both strategies would provide maximum protection, especially for extremely short cloud arrival times.

The data from this DSS can help design a methodology for early warning system placement for both strategies. The large amount of data generated on cloud spread trajectories from all NPPs can be used to place measuring stations based on detection rate, cost constraints, and other factors. This method would be advantageous when cost optimization is a key constraint. To the best of the author’s knowledge, no such methodology exists in the literature.

REFERENCES

Airport Technology. Hamad International Airport (HIA). https://www.airport-technology.com/projects/doha/, Accessed 2021

Al-Mulla, Y., 2006. Cooling Greenhouses in the Arabian Peninsula. Acta horticulturae, 719, 499-506.

Al-Qaradawi, I., Abdel-Moati, M., Al-Yafei, M.A.-A., Al-Ansari, E., Al-Maslamani, I., Holm, E., Al-Shaikh, I., Mauring, A., Pinto, P.V., Abdulmalik, D., Amir, A., Miller, M., Yigiterhan, O.,Persson, B., 2015. Radioactivity levels in the marine environment along the Exclusive Economic Zone (EEZ) of Qatar. Marine Pollution Bulletin, 90, 323-329.

Al-Siddiqi, A.,Dawe, R. (1998). A Review Of Petroleum Engineering Aspects Of Qatar's Oil And Gas.

Al-Thani, A., Afifi, N., Fthenou, E., Hannigan, L., Mostafa, M.B.M.A.,Kasem, M.M., 2017a. Qatar Biobank Report 2016-2017. Qatar: Qatar Biobank.

Al-Thani, M., Al-Thani, A.A., Al-Mahdi, N., Al-Kareem, H., Barakat, D., Al-Chetachi, W., Tawfik, A.,Akram, H., 2017b. An Overview of Food Patterns and Diet Quality in Qatar: Findings from the National Household Income Expenditure Survey. Cureus, 9.

Al Jazeera. (2021). Qatar announces new restrictions amid fears of second COVID wave. *Al Jazeera*.

Alexakhin, R.M., 1993. Countermeasures in agricultural production as an effective means of mitigating the radiological consequences of the Chernobyl accident. Science of The Total Environment, 137, 9-20.

Aliyu, A.S., Ramli, A.T.,Saleh, M.A., 2014. Environmental impact assessment of a new nuclear power plant (NPP) based on atmospheric dispersion modeling. Stochastic Environmental Research and Risk Assessment, 28, 1897-1911.

Aliyu, A.S., Ramli, A.T.,Saleh, M.A., 2015. Assessment of potential human health and environmental impacts of a nuclear power plant (NPP) based on atmospheric dispersion modeling. Atmósfera, 28, 13-26.

Alkhalidi, A., Khawaja, M.K.,Abusubaih, D., 2020. Energy efficient cooling and heating of aquaponics facilities based on regional climate. International Journal of Low-Carbon Technologies, 15, 287-298.

Andrade, A.,Dominski, F.H., 2018. Indoor air quality of environments used for physical exercise and sports practice: Systematic review. J Environ Manage, 206, 577-586.

Andronopoulos, S., Davakis, E.,Bartzis, J.G., 2002. RODOS-DIPCOT Model Description and Evaluation (No. RODOS(RA2)-TN(09)-01).

ARGOS, 2014. PDC Argos: CBRN Crisis Management. Argos. https://pdc-argos.com/. Retrieved 1st January 2020, Accessed 2020

Arora, R., Chawla, R., Marwah, R., Kumar, V., Goel, R., Arora, P., Jaiswal, S.,Sharma, R.K., 2010. Medical radiation countermeasures for nuclear and radiological emergencies: Current status and future perspectives. J Pharm Bioallied Sci, 2, 202-212.

Beeley, P.A.,Kim, S.-Y. (2014). Preliminary Radioactive Dispersion Modeling in the Arabian Gulf
Using the ADMS-5 Gaussian Plume Model, *Peaceful Use of Nuclear Energy and Its Impact on Environmental Security*. Bahrain: Royal College of Bahrain Police.

Brown, J., Mortimer, K., Andersson, K.G., Duranova, T., Mrskova, A., Hänninen, R., Ikäheimonen, T., Kirchner, G., Bertsch, V., Fallay, F.,Reales, N., 2007. Generic handbook for assisting in the management of contaminated inhabited areas in Europe following a radiological emergency. Didcot: Health Protection Agency.

Brumfiel, G. (2019). As Saudi Arabia Builds A Nuclear Reactor, Some Worry About Its Motives. *NPR*.

Burdon-Manley, L. (2017). Qatari farmers trying to find new ways to increase production. *Al Jazeera*.

Castelier, S. (2019). Qatar's agriculture push risks further groundwater depletion. *Al-Monitor*.

Chino, M., Ishikawa, H.,Yamazawa, H., 1993. SPEEDI and WSPEEDI: Japanese emergency response systems to predict radiological impacts in local and workplace areas due to a nuclear accident. Radiation Protection Dosimetry, 50, 145-152.

Crystal, J.A.,Anthony, J.D. (2021). Qatar, *Britannica*.

Datablog. (2011). Nuclear power plant accidents: listed and ranked since 1952. *The Guardian, .*

Dinno, A., 2015. Nonparametric Pairwise Multiple Comparisons in Independent Groups using Dunn's Test. The Stata Journal, 15, 292-300.

Dombrowski, H., Bleher, M., Cort, M.D., Dabrowski, R., Neumaier, S.,Stöohlker, U., 2017. Recommendations to harmonize European early warning dosimetry network systems. Journal of Instrumentation, 12, P12024-P12024.

Dvorzhak, A., Mora, J.C.,Robles, B., 2016. Probabilistic risk assessment from potential exposures to the public applied for innovative nuclear installations. Reliability Engineering & System Safety, 152, 176-186.

Ebel, E.R., 2010. Geopolitics of the Iranian Nuclear Energy Program: But Oil and Gas Still Matter (CSIS Reports): Center for Strategic & International Studies.

Eckerman, K., Harrison, J., Menzel, H.G.,Clement, C.H., 2013. ICRP Publication 119: Compendium of Dose Coefficients based on ICRP Publication 60. Annals of the ICRP, 42.

Ehrlenbruch, R., Eknæs, M., Pollen, T., Andersen, I.L.,Bøe, K.E., 2010. Water intake in dairy goats - the effect of different types of roughages. Italian Journal of Animal Science, 9.

Emirates Nuclear Energy Corporation, 2018. Final Dome Structure Completed at Barakah Nuclear Energy Plant. https://www.enec.gov.ae/news/latest-news/final-dome-structure-completed-at-barakah-nuclear-energy-plant/#:~:text=The, Accessed 2020

FAO/IIASA/ISRIC/ISSCAS/JRC. (2012). Harmonized World Soil Database (version 1.2). FAO, Rome, Italy and IIASA, Laxenburg, Austria.

FEMA. (2010). Developing and Maintaining Emergency Operations Plans (Vol. 2).

Fesenko, S., Jacob, P., Ulanovsky, A., Chupov, A., Bogdevitch, I., Sanzharova, N.I., Kashparov, V., Panov, A.,Zhuchenka, Y., 2010. Justification of remediation strategies in the long term after the Chernobyl accident. Journal of environmental radioactivity, 119.

FT Visual & Data Journalism Team. (2021). Lockdowns compared: tracking governments' coronavirus responses. *Financial Times*.

Funabashi, Y.,Kitazawa, K., 2012. Fukushima in review: A complex disaster, a disastrous response. Bulletin of the Atomic Scientists, 68, 9-21.

Gering, F., Raskob, W.,Charnock, T., 2010. New model for agricultural countermeasures in RODOS and ARGOS. http://dx.doi.org/10.1051/radiopro/2010035, 45.

Gulf Labour Markets and Migration, 2017, December 2017. Qatar: Population by nationality (Qatari/ non-Qatari) at dates/ years of census (1970-2015. https://gulfmigration.org/qatar-population-by-nationality-qatari-non-qatari-at-dates-years-of-census-1970-2015/. Retrieved 20th August 2020, Accessed 2020

Gyamfi, K., Birikorang, S.A., Ampomah-Amoako, E.,Fletcher, J.J., 2020. Radiological Safety Analysis for a Hypothetical Accident of a Generic VVER-1000 Nuclear Power Plant. Science and Technology of Nuclear Installations, 2020, 1-8.

Hankin, D.G., Mohr, M.S.,Newman, K.B., 2019. Sampling Theory : For the Ecological and Natural Resource Sciences. Oxford, UNITED KINGDOM: Oxford University Press USA - OSO.

Hassan, H., Saraga, D., Kumar, P.,Kakosimos, K.E., 2020. Vehicle-induced fugitive particulate matter emissions in a city of arid desert climate. Atmospheric Environment, 229.

I.V, V.n.,Lemeshko, B., 2014. The analytical review of tests for randomness and the absence of a trend.

IAEA, 2016. Criteria for radionuclide activity concentrations for food and drinking water. Vienna.

IAEA,FAO, 2020. Strategies and Practices in the Remediation of Radioactive Contamination in Agriculture : Report of a Technical Workshop in Vienna, Austria, 17–18 October 2016. Vienna: IAEA.

Ievdin, I., Khalchenkov, A., Raskob, W., D.M, T., Zheleznyak, M.,Kovalets, I., 2012. Application of Decision Support system JRODOS for assessments of atmospheric dispersion and deposition from Fukushima Daiichi Nuclear Power Plant accident. International Journal of Energy for a Clean Environment, 13, 179-190.

Ievdin, I., Landman, C., Päsler-Sauer, J.,Staudt, C. (2019a). Result Guide for the models in the JRodos Emergency Model Chain V3.0.

Ievdin, I., Trybushny, D., Zheleznyak, M.,Raskob, W., 2010. RODOS re-engineering: Aims and implementation details. http://dx.doi.org/10.1051/radiopro/2010024, 45.

Ievdin, I., Trybushnyi, D., Landman, C.,Staudt, C., 2019b. JRodos User Guide V4.0: Karlsruher Institute of Technology,.

Jafarikia, S.,Feghhi, S.A.H., 2018. Study of in-containment source term behavior for VVER-1000 under LOCA conditions using the IRBURN code system. Annals of Nuclear Energy, 112, 17-29.

Johnson, S. (2018). Middle East countries plan to add nuclear to their generation mix: US Energy Information Administration.

Joyce, M. (2018). Chapter 14 - Nuclear Safety and Regulation. In M. Joyce (Ed.), *Nuclear Engineering* (pp. 323-355): Butterworth-Heinemann.

Karanisa, T., Amato, A., Richer, R., Abdul Majid, S., Skelhorn, C.,Sayadi, S., 2021. Agricultural Production in Qatar's Hot Arid Climate. Sustainability, 13.

KEPCO. APR1400. KEPCO. https://www.kepco-enc.com/eng/contents.do?key=1533, Accessed 2020

Kirichenko, V.A., Kirichenko, A.V.,Werts, D.E., 2012. Consequences and countermeasures in a nuclear power accident: Chernobyl experience. Biosecur Bioterror, 10, 314-320.

LAKA Foundation. IAEA-database of nuclear and radiological incidents. https://www.laka.org/docu/ines/, Accessed 2021

Lerner, R., 2000. What is Loam? Purdue University Consumer Horticulture. https://www.purdue.edu/hla/sites/yardandgarden/what-is-loam/. Retrieved 20th August 2020, Accessed 2020

Li, J.X., Cao, X.W., Tong, L.L.,Huang, G.F., 2012. Radiological consequence evaluation of DBAs with alternative source term method for a Chinese PWR. Nuclear Engineering and Design, 250, 260-266.

Liland, A., Lind, O.C., Bartnicki, J., Brown, J.E., Dyve, J.E., Iosjpe, M., Klein, H., Lin, Y., Simonsen, M., Strand, P., Thorring, H., Ytre-Eide, M.A.,Salbu, B., 2020. Using a chain of models to predict health and environmental impacts in Norway from a hypothetical nuclear accident at the Sellafield site. J Environ Radioact, 214-215, 106159.

Lim, L.L., Hughes, S.J.,Hellawell, E.E., 2005. Integrated decision support system for urban air quality assessment. Environmental Modelling & Software, 20, 947-954.

Maderich, V., Bezhenar, R., Tateda, Y., Aoyama, M., Tsumune, D., Jung, K.T.,de With, G., 2018. The POSEIDON-R compartment model for the prediction of transport and fate of radionuclides in the marine environment. MethodsX, 5, 1251-1266.

Mannan, M., Alhaj, M., Mabrouk, A.N.,Al-Ghamdi, S.G., 2019. Examining the life-cycle environmental impacts of desalination: A case study in the State of Qatar. Desalination, 452, 238-246.

Marusteri, M.,Bacarea, V., 2009. Comparing groups for statistical differences: how to choose the right statistical test?

Mascarenhas, S., 2014. The Arabian Legend. Marhaba Qatar Destination Guide. https://www.marhaba.qa/the-arabian-legend/#:~:text=These%20horses%20weigh%20between%20800,black%20or%20roan%20in%20colour.

Mateus, A.,Caeiro, F., 2014. An R implementation of several randomness tests. AIP Conference Proceedings, 1618, 531-534.

McKenna, T.J.,Glitter, J.G. (1988). Source Term Estimation During Incident Response to Severe Nuclear Power Plant Accidents. Washington, DC.

Mehboob, K., Park, K.,Khan, R., 2015. Quantification of in-containment fission products source term for 1000 MWe PWR under loss of coolant accident. Annals of Nuclear Energy, 75, 365-376.

Mehboob, K.,Xinrong, C., 2012. Source term evaluation of two loop PWR under hypothetical severe accidents. Annals of Nuclear Energy, 50, 271-284.

Min, J.S.,Kim, H.R., 2018. Environmental impact on the Korean peninsula due to hypothetical accidental scenarios at the Haiyang nuclear power plant in China. Progress in Nuclear Energy, 105, 254-262.

Ministry of Development Planning and Statistics, 2013. Final Results of Household Expenditure and Income Survey (HEIS). Doha.

Mohammed Saeed, I.M., Saleh, M.A.M., Hashim, S., Hama, Y.M.S., Hamza, K.,Al-Shatri, S.H., 2020. The radiological assessment, hazard evaluation, and spatial distribution for a hypothetical nuclear power plant accident at Baiji potential site. Environmental Sciences Europe, 32.

Müller, H., Gering, F.,Pröhl, G., 2003. Model Description of the Terrestrial Food Chain and Dose Module FDMT in RODOS PV6.0 RODOS (No. RODOS(RA3)-TN(03)06): GSF - Institut für Strahlenschutz.

Nasstrom, J.S., Sugiyama, G., Baskett, R.L., Larsen, S.C.,Bradley, M.M., 2007. The National Atmospheric Release Advisory Center modelling and decision-support system for radiological and nuclear emergency preparedness and response. International Journal of Emergency Management, 4.

Nayak, B.K.,Hazra, A., 2011. How to choose the right statistical test? Indian journal of ophthalmology, 59, 85-86.

NERIS, 2016, 31 May 2016. HARMONE. https://www.eu-neris.net/projects/operra/operra-harmone.html. Retrieved 18 August 2020, Accessed 2020

NOAA. Global Forecast System (GFS). NOAA. https://www.ncdc.noaa.gov/data-access/model-data/model-datasets/global-forcast-system-gfs. Retrieved 08 August 2020, Accessed 2020

Päsler-Sauer, J., 2010. Comparison and validation exercises of the three atmospheric dispersion models in RODOS. Radioprotection, 45, S89-S96.

Pasquill, F. (1961). The estimation of the dispersion of windborne material. *The Meteorological Magazine, 90,* 33-49.

Pirouzmand, A., Dehghani, P., Hadad, K.,Nematollahi, M., 2015. Dose assessment of radionuclides dispersion from Bushehr nuclear power plant stack under normal operation and accident conditions. International Journal of Hydrogen Energy, 40, 15198-15205.

Planning & Statistics Authority, 2017a. Agricultural Statistics. Doha.

Planning & Statistics Authority, 2017b. Water statistics in the state of Qatar. Doha: Planning & Statistics Authority - State of Qatar.

Planning & Statistics Authority, 2018. Qatar Economic Outlook 2018-2020. Qatar.

Poon, C.B., Au, S.M., Prohl, G.,Muller, H., 1997. Adaptation of Ecosys-87 to Hong Kong Environmental Conditions. Health Physics, 72, 856-864.

Powers, A.B., 2010. Stratified Random Sampling (4th ed.): Springer Publishing Company.

Qatar Blocks and Fields (2014). *The Oil & Gas Year Qatar 2014*.

Qatar Petroleum. Halul Island. https://www.qp.com.qa/en/QPActivities/QPOperations/Pages/IndustrialCitiesDetails.aspx?IID=5, Accessed 2020

Raisali, G., Davilu, H., Haghighishad, A., Khodadadi, R.,Sabet, M., 2006. Calculation of total effective dose equivalent and collective dose in the event of a LOCA in Bushehr Nuclear Power Plant. Radiat Prot Dosimetry, 121, 382-390.

Raja Shekhar, S.S., Venkata Srinivas, C., Rakesh, P.T., Deepu, R., Prasada Rao, P.V.V., Baskaran, R.,Venkatraman, B., 2020. Online Nuclear Emergency Response System (ONERS) for consequence assessment and decision support in the early phase of nuclear accidents - Simulations for postulated events and methodology validation. Progress in Nuclear Energy, 119.

Raskob, W., Landman, C.,Trybushnyi, D. JRODOS : Real-time online decision support system for nuclear emergency management: Karlsruhe Institute of Technology.

Raskob, W., Landman, C.,Trybushnyi, D., 2016. Functions of decision support systems (JRodos as an example): Overview and new features and products. Radioprotection, 51, S9-S11.

Segal, M.G., 1993. Agricultural countermeasures following deposition of radioactivity after a nuclear accident. Science of The Total Environment, 137, 31-48.

Shakespeare, A. (2014). Industrial cities in Qatar. *MEED*.

Shamsuddin, S.D., Koh, M.H., Basri, N.A., Omar, N., Koh, M.-H., Ramli, A.T., Saridan Wan Hassan, W.M., Krishnan, G.,Mohd Noor, F., 2017. Radioactive dispersion analysis for hypothetical nuclear power plant (NPP) candidate site in Perak state, Malaysia. EPJ Web of Conferences, 156.

Shinano, T., 2016. Mitigation of Radioactive Contamination from Farmland Environment and Agricultural Products. Modern Environmental Science and Engineering, 2, 454-461.

Smith, J.T., Voitsekhovitch, O.V., Håkanson, L.,Hilton, J., 2001. A critical review of measures to reduce radioactive doses from drinking water and consumption of freshwater foodstuffs. J Environ Radioact, 56, 11-32.

Soffer, L., Burson, S.B., Ferrell, C.M., Lee, R.Y.,Ridgely, J.N. (1995). Accident Source Terms for Light-Water Nuclear Power Plants. Washington, DC.

Sohrabi, M., Ghasemi, M., Amrollahi, R., Khamooshi, C.,Parsouzi, Z., 2013a. Assessment of environmental public exposure from a hypothetical nuclear accident for Unit-1 Bushehr nuclear power plant. Radiat Environ Biophys, 52, 235-244.

Sohrabi, M., Parsouzi, Z., Amrollahi, R., Khamooshy, C.,Ghasemi, M., 2013b. Public exposure from environmental release of radioactive material under normal operation of unit-1 Bushehr nuclear power plant. Annals of Nuclear Energy, 55, 351-358.

Soil Survey Division Staff, 1993. Soil Survey Manual: United States Department of Agriculture.

Syrakov, D., Prodanova, M.,Slavov, K., 2003. Description and performance of Bulgarian Emergency Response System in case of nuclear accident (BERS). International Journal of Environment and Pollution, 20, 286-296.

Taleb, N.N., 2007. The Black Swan: The Impact of the Highly Improbable: Penguin.

Tang, Z., Cai, J., Li, Q., Zhao, J., Li, X.,Yang, Y., 2020. The regional scale atmospheric dispersion analysis and environmental radiation impacts assessment for the hypothetical accident in Haiyang nuclear power plant. Progress in Nuclear Energy, 125.

Thykier-Nielsen, S., Deme, S.,Mikkelsen, T., 1999. Description of the Atmospheric Dispersion Module RIMPUFF (No. RODOS(WG2)-TN(98)-02).

Time and Date AS. 2017 Sun Graph for Bushehr. https://www.timeanddate.com/sun/iran/bushehr?month=5&year=2017, Accessed 2021

Toumi, H. (2010). Summer in Qatar is hottest on record. *Gulf News*.

U.S. Environmental Protection Agency, 1989. Report to Congress on indoor air quality. Volume 2. Assessment and control of indoor air pollution. Final report (No. U.S. Environmental Protection Agency). United States.

UAE Federal Authority for Nuclear Regulation, 2012. Safety Evaluation Report of an Application for a Licence to Construct Barakah Units 1 and 2. Abu Dhabhi: FANR.

UAE Federal Authority for Nuclear Regulation, 2014. Safety Evaluation Report of an Application for a Licence to Construct Barakah Units 3 and 4. Abu Dhabhi: FANR.

United States Department of Agriculture. Soil Texture Calculator. https://www.nrcs.usda.gov/wps/portal/nrcs/detail/soils/survey/?cid=nrcs142p2_054167. Retrieved August 20, 2020, Accessed 2020

USNRC. (2018). Subpart D—Radiation Dose Limits for Individual Members of the Public.

Vaiserman, A., Koliada, A., Zabuga, O.,Socol, Y., 2018. Health Impacts of Low-Dose Ionizing Radiation: Current Scientific Debates and Regulatory Issues. Dose-Response, 16, 1559325818796331.

Walker, L. (2016). Qatar's Hamad Port to become fully operational this week. *Doha News*.

Ward, D.,McKague, K. (2019). Water Requirements of Livestock: Ontario Ministry of Agriculture, Food and Rural Affairs, .

Weglarczyk, S., 2018. Kernel density estimation and its application. ITM Web of Conferences, 23.

Wengert, A., 2017. JRodos: An off-site emergency management system for nuclear accidents Karlsruhe Institute of Technology (KIT).

WHO, 2016. Ionizing radiation, health effects and protective measures. https://www.who.int/news-room/fact-sheets/detail/ionizing-radiation-health-effects-and-protective-measures

WHO,FAO, 2011. Nuclear accidents and radioactive contamination of foods.

World Integrated Trade Solution. Qatar Food Products Imports By Country 2017. https://wits.worldbank.org/CountryProfile/en/Country/QAT/Year/2017/TradeFlow/Import/Partner/by-country/Product/16-24_FoodProd. Retrieved May 16 2021, Accessed 2021

World Nuclear Association, 2019, May 2019. Nuclear Power in Saudi Arabia. https://www.world-nuclear.org/information-library/country-profiles/countries-o-s/saudi-arabia.aspx

World Nuclear Association, 2020a, June 2020. Nuclear Power in Iran. World Nuclear Association. https://www.world-nuclear.org/information-library/country-profiles/countries-g-n/iran.aspx

World Nuclear Association, 2020b, November 2020. Nuclear Power in the United Arab Emirates. World Nuclear Association. https://www.world-nuclear.org/information-library/country-profiles/countries-t-z/united-arab-emirates.aspx

World Nuclear Association, 2020c. Nuclear Radiation and Health Effects. https://www.world-nuclear.org/information-library/safety-and-security/radiation-and-health/nuclear-radiation-and-health-effects.aspx

Yatsalo, B., 2007. Decision support system for risk-based land management and rehabilitation of radioactively contaminated territories: PRANA approach. International Journal of Emergency Management, 4.

Yatsalo, B., Mirzeabassov, O., Okhrimenko, I., Pichugina, I.,Kulagin, B., 1997. PRANA - Decision Support System for Assessment of Countermeasure Strategy in the

Long-Term Period of Liquidation of the Consequences of a Nuclear Accident (Agrosphere). Radiation Protection Dosimetry, 73, 291-294.

Ytre-Eide, M., Standring, W., Amundsen, I., Sickel, M., Liland, A., Saltbones, J., Bartnicki, J., Haakenstad, H.,Salbu, B., 2009. Consequences in Norway of a hypothetical accident at Sellafield : potential release – transport and fallout.

Yu, C.-Y., Lin, C.-H.,Yang, Y.-H., 2010. Human body surface area database and estimation formula. Burns, 36, 616-629.

Zehringer, M. (2016). Radioactivity in Food: Experiences of the Food Control Authority of Basel-City since the Chernobyl Accident.

APPENDIX A

ASSUMPTIONS USED IN PREPROCESSING OF RECEPTOR DATA

List of Receptors

The list of secondary receptors used in this project is shown in Table 4 below. The agricultural receptor type was not split further due to the absence of data.

Table 4: Secondary receptors used in this study

Type	Name
Agriculture	Agriculture
City	Al Wakra
	Dukhan
	Al Khor
	Industrial Area
	Rayyan
	Doha
Desalination Plant	Ras Abu Fontas
	Umm Al Houl
	Dukhan Desalination
Gas Field	North Oil Field
Industry	Mesaieed
	Ras Laffan
Oil Field	Shaheen Oil Field
	Al Khalij Oil Field
	Bul Hanine
	Idd El Shargi
	Maydan Mahzam
	Al Rayyan Field
	Al Karkara
	A- Structure
	Al- Bunduq
	Dukhan Oil Field
Transport Hub	HIA
	Hamad Port
Halul Island	Halul Island

Land Use & Soil Classification

One combined map was obtained for Qatar's land use and soil classification (Hassan et al., 2020). The original data had a different format for classification compared to the expected JRODOS input. JRODOS classifies land use as agricultural, forest, urban, water, and grassland/undefined. On the other hand, JRODOS categorizes soil as peaty, sandy, loamy, clay, and no data. QGIS was used to split the original data into two maps for JRODOS use. Then, the data conversion was done, as shown in Table 5 below.

Table 5: Reclassification of land use & soil map JRODOS classifications

Original	JRODOS Land use	JRODOS Soil
Industrial	Urban	Clay
Urban & built-up	Urban	Loam
Rangeland	Agricultural	Loam
Water	Water	No data
Barren land (Soil type: Solonchaks)	Grassland/Undefined	Clay
Barren land (Soil type: Sand Dunes)	Grassland/Undefined	Sand
Barren land (Soil type: Leptosols)	Grassland/Undefined	Loam
Barren land (Soil type: Calcisols/in city)	Grassland/Undefined	Loam
Barren land (Soil type: Calcisols/out city)	Grassland/Undefined	Loam

As seen in Table 5 above, the reclassification of land use is relatively straightforward. Industrial areas were also assumed to be urban as they most resemble urban regions in infrastructure and population distribution.

The reclassification of the soil map was a more involved process. The reclassification was done using the USDA soil texture triangle. The sand, clay, and silt composition for the four soil types mentioned above in Table 5 were obtained from the

harmonized world soil database by FAO and IIASA and are shown in Table 6 below (FAO/IIASA/ISRIC/ISSCAS/JRC, 2012).

Table 6: Composition of soil types in Qatar based on harmonized world soil database (FAO/IIASA/ISRIC/ISSCAS/JRC, 2012)

Soil Type	Sand	Silt	Clay
Calcisols	51	31	19
Solonchaks	31	35	34
Leptosols	41	36	24
Sand Dunes	86	9	6

These classifications were used to reclassify the soil types into sandy, clay, and loamy based on the soil texture triangle from USDA, as shown in Figure 21 below (United States Department of Agriculture; Soil Survey Division Staff, 1993). The rangelands (agricultural areas) were assumed to be loamy since loamy soil is more fertile than clay or sandy soil (Lerner, 2000). No peat was assumed for Qatar because peat is typically found in wet climates with a lot of organic matter such as trees shrubs, and other flora (Soil Survey Division Staff, 1993). The industrial and urban areas were assumed to be the same soil type as the predominant soil type surrounding them.

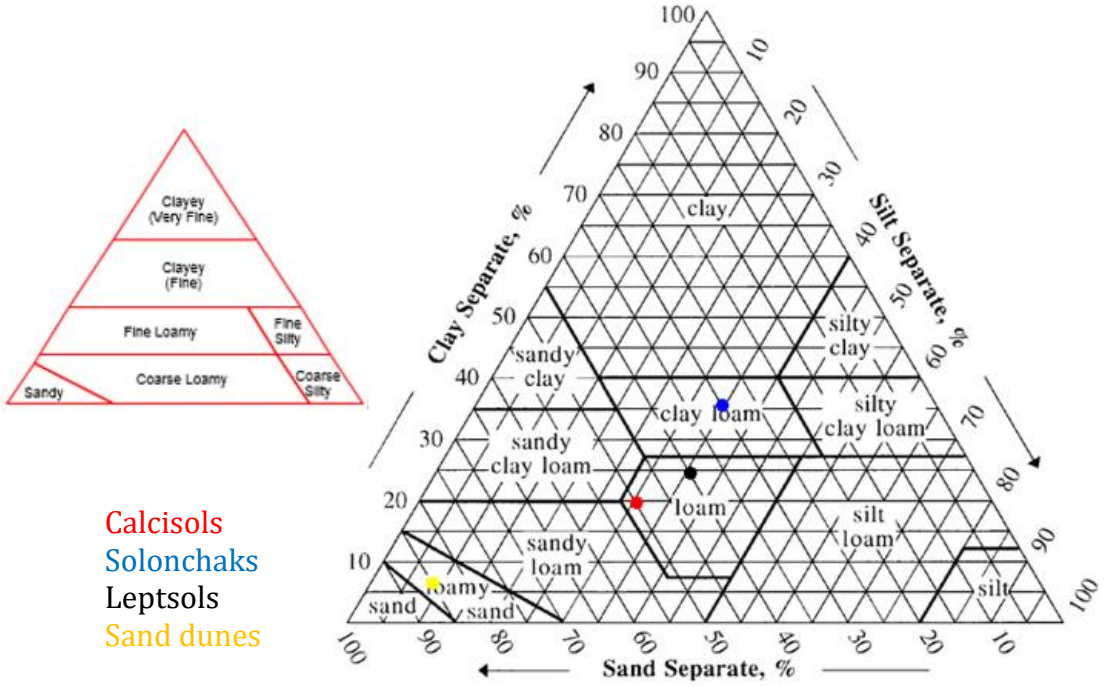

Figure 21: Reclassification of Soil Map based on USDA Soil Texture Triangle (United States Department of Agriculture)

Food Consumption

The food consumption rates available from MDPH were monthly household rates for Qataris and non-Qataris separately (Ministry of Development Planning and Statistics, 2013). This rate was converted into an individual daily rate using the average household size provided within the same survey. A weighted average based on the distribution of Qataris and Non-Qataris within Qatar (Gulf Labour Markets and Migration, 2017) was used to estimate a unified daily individual consumption rate for each foodstuff.

All food consumption rates were scaled down based on the local agricultural production rate for the specific food (Planning & Statistics Authority, 2017a). In many

cases, the percentage of food produced locally was only available in terms of the primary foodstuff classification such as vegetable, fruit, milk products, and not specific products. In these cases, the uniform scaling factor was assumed for all products under the main category. For example, 16% of vegetables were produced locally. Thus food consumption of root, leafy, and other vegetables was scaled down evenly by 16%.

These imported foods are considered safe from any fallout from NPP accidents within the GCC. Additionally, the following assumptions were made as part of preprocessing for us in JRODOS:

- Wheat is available and grown within Qatar in spring and winter. This assumption was made based on Qatar's growing nearly all of its food within greenhouses that are less dependent on climate. (Burdon-Manley, 2017)
- One-fourth of all wheat products were assumed to be whole wheat and the rest as typically processed wheat
- All beef consumed was assumed to be cow meat and not bull or veal meat
- All milk consumed was assumed to be cow milk
- No seasonal intake factors were applied to different foodstuffs as Qatar imports most of its food (Planning & Statistics Authority, 2017a).
- Cheese consumed local was assumed to be 50% rennet type and 50% acidic type
- Any vegetable not classified as root or leafy vegetable was classified as fruit vegetable. For example, the tomato was considered a fruit vegetable.

- Consumption rates for vegetables only classified as "frozen", "fresh "or "canned" without specific vegetable names were divided into three parts and added to consumption rates of root, leafy, and fruit vegetables each.
- Dates were not classified as fruits

The food consumption rates derived by the above methodology and used for estimation of the ingestion radiation dose are shown below in Table 7.

Table 7: Contaminable food input for JRODOS calculations

Foods	Total adult food intake (g/day)	%Self Sufficiency	Contaminable food intake (g/day)
Whole Wheat (Whole)	48	3.4%	1.6
Wheat Flour	193	3.4%	6.5
Potato	63	16.4%	10.3
Leafy veg	70	16.4%	11.6
Root veg	179	16.4%	29.3
Fruit veg	89	16.4%	14.6
Fruits *	316	0.5%	1.5
Berries	0	16.4%	0.0
Milk	148	26.8%	39.7
Cond Milk	55	26.8%	14.7
Cream	37	26.8%	9.9
Butter	5	26.8%	1.4
Cheese (ren.)	10	26.8%	2.7
cheese (acid)	10	26.8%	2.7
Sheep milk	0	26.8%	0.0
Goat milk	0	26.8%	0.0
Beef (cow)	29	13.2%	3.8
Lamb	56	13.2%	7.4
Chicken	73	9.5%	7.0
Eggs	42	13.6%	5.7
Fish	40	31.7%	12.5
* The daily food intake for fruits is 305 g/day. Instead, food intake of 316.1 g/day is for fruits + dates, of which a total of 13.1% is produced locally. Thus, the fruits contaminable food intake should have been 1.4 g/day			

Agricultural Production

The following assumptions were made regarding crops while using the available agricultural production data:

- Wheat and barley are grown both in spring and winter.
- One-fourth of all wheat gown is processed to be whole wheat, and the rest is assumed to be regular wheat flour.
- Half of the green fodder was assumed to be grass and the other half as hay

No direct information was available on the feed water given to animals. However, the number of animals reared within Qatar in 2017 was available (Planning & Statistics Authority, 2017a). This information was combined with the average daily water intake data for each animal to obtain the overall feed water consumption rates shown in Table 8.

Table 8: Feedwater consumption rates for animals reared in Qatar in 2017

Animals	Number of Animals (Planning & Statistics Authority, 2017a)	Water consumed per animal daily (L/day*animal) (Ehrlenbruch et al., 2010; Ward and McKague, 2019)	Water consumed annually (m3/year)
Cows	24958	155.00	1.41E+06
Sheep	932472	8.14	2.77E+06
Goats	382423	7.90	1.10E+06
Camels	105387	39.00	1.50E+06
Horses	7333	39.00	1.04E+05
Poultry	10524315	0.73	2.80E+06
		Sum	9.69E+06

\The following assumptions were made while deriving the annual water consumption rate:

- The maximum water consumption rate was used as Qatar's hot climate necessitates a higher water consumption rate
- All cows were assumed to be of the Holstein variety as most local cows are of the Holstein variety. While 700 liters are used per cow in Qatar, most of this is misting to control the temperature (Castelier, 2019). As a result, the cow only consumes around 155 liters (Ward and McKague, 2019). Thus, the water consumption rate was calculated based on the 155-liter consumption rate.
- The exact distribution of sheep between feeder lambs, ewes, etc., was not known. Thus, the feed rates of sheep throughout all stages of life were averaged to determine the water consumption rate
- The local breed of horses was assumed to be all Arabian horses with an average weight of 800-1000 pounds (Mascarenhas, 2014).
- Camel water consumption was assumed to be the same as a horse in the absence of data.
- The water consumption rate of poultry in fall, spring, winter, and summer was averaged to derive a daily water consumption rate.

Skin Area

The average skin area was estimated using the formulation proposed by Yu et al.. This formula was obtained by studying 135 people of each gender using 3D body surface scans and was shown to have a smaller estimation error than the standard procedures used nowadays, such as the Du Bois and Du Bois formula. The formula is shown in Eq. 3 below (Yu et al., 2010).

$$BSA(cm^2) = 71.3989 \times H(cm)^{0.7437} \times W(kg)^{0.4040} \quad \text{Eq. 3}$$

Where BSA is Body surface area (cm^2)

H is height (cm)

W is weight (kg)

Height and weight data for men and women in Qatar from Qatar biobank (Al-Thani et al., 2017a) were used to obtain an average skin area of 1.87 $m^{2,}$ as shown in Table 9 below.

Table 9: Height, Weight and Skin Area of Men & Women within Qatar

	Men	**Women**
Height (cm) (Al-Thani et al., 2017a)	172.60	158.00
Weight (kg) (Al-Thani et al., 2017a)	85.90	73.90
Skin Area(m^2)	1.99	1.75
Average Skin Area (m^2)	1.87	

APPENDIX B

DETAILS OF SELECTED NUCLEAR PLANTS

Iran

Iran currently has one operational nuclear plant, Bushehr. The reactor has one unit, with details in Table 10 below. Plans are in place to expand the Bushehr plant in four phases and build nuclear plants at other sites like Makran coast (World Nuclear Association, 2020a).

Table 10: Details of the Reactor at Bushehr Nuclear Power Plant in Iran (Jafarikia and Feghhi, 2018; World Nuclear Association, 2020a)

Reactor Model	VVER-1000/V-446 (PWR)
Thermal power production (MWt)	1 x 3000
Electrical power production (MWe)	1 x 915
Startup Date	May 2011
Commercial Operation	September 2013
Containment Chamber Dimension	56 m (Spherical)

UAE

UAE is building one nuclear power plant, Barakah, in collaboration with South Korea. The reactor has four identical units, with their details given in Table 11 below.

Table 11: Details of the Reactor at Barakah Nuclear Power Plant in UAE (UAE Federal Authority for Nuclear Regulation, 2012, 2014; World Nuclear Association, 2020b)

Reactor Model	APR-1400 (PWR)
Thermal power production (MWt)	4000
Electrical power production (MWe)	4 x 1390
Startup Date	August 2020 (Reactor 1)
Commercial Operation	--
Containment Chamber Dimension	70 m (Dome height)

KSA

KSA currently has no commercial operating reactors, and none are under construction. However, KSA has committed to developing local nuclear power generation capability. Towards this end, it has signed agreements with several companies to explore reactor technologies. Some of the larger reactor units considered are GE Hitachi's ESBWR, Toshibas ABWR, and Toshiba/Westinghouse's AP1000. The first two are boiling water reactors (BWR), with the last being a PWR. In addition, two smaller reactors are also being considered. The first is the South Korean SMART reactor, and the second is the Chinese High-Temperature Reactors (HTR) (World Nuclear Association, 2019). However, KSA has one research reactor under contruction in Riyadh(Brumfiel, 2019).

APPENDIX C

FOOD GUIDELINE LEVELS

The calculated guideline is shown in Table 12 below, with the lowest GL level for each radionuclide in bold.

Table 12: Guideline values for iodine contamination of food

	I-131	**I-132**	**I-133**	**I-134**	**I-135**	
Adult Dose Factor (Sv/Bq)	2.20E-08	2.90E-10	4.30E-09	1.10E-10	9.30E-10	
Guideline Level (Bq /kg)	**620**	47043	3173	124023	14669	
	Cs-134	**Cs-134m**	**Cs-135m**	**Cs-136**	**Cs- 137**	**Cs-138**
Adult Dose Factor (Sv/Bq)	1.90E-08	2.00E-11	1.90E-11	3.00E-09	1.30E-08	9.20E-11
Guideline Level (Bq /kg)	**718**	682128	718030	4548	1049	148289

Finally, the median contamination value for each food is shown in Table 13 below. JRODOS did not calculate cesium contamination for lamb.

Table 13: Food guideline used in this study for selection of foods to mitigate

Foods	Iodine median Contamination (Bq/ kg)	Cesium median Contamination (Bq/ kg)
Acidic Cheese	53.55	7.46
Beef	0.45	19.97
Butter	30.51	3.00
Chicken	0.22	5.39
Condensed Milk	96.87	29.06
Cream	44.82	9.23
Eggs	106.55	5.53
Fruits	110.33	1.48
Lamb	0.021	--
Leafy veg	18286.37	8604.48
Milk	69.66	12.86
Other Veg	28.59	0.48
Potato	56.97	0.47
Rennet Cheese	4.79	7.81
Root veg	72.12	0.95